Journal of Pharmaceutical Analysis 15 (2025) 101042

Contents lists available at ScienceDirect

Journal of Pharmaceutical Analysis

journal homepage: www.elsevier.com/locate/jpa

Original article

Phillygenin ameliorates tight junction proteins reduction, fibrosis, and apoptosis in mice with chronic colitis via TGR5-mediated PERK-eIF2α-Ca^{2+} pathway

Huanhuan Xue [a, b], Peijie Li [a, b], Jing Guo [c], Tinggui Chen [a], Shifei Li [a, **], Liwei Zhang [a, *]

[a] Institute of Molecular Science, Key Laboratory of Chemical Biology and Molecular Engineering of Ministry of Education, Shanxi University, Taiyuan, 030006, China
[b] Modern Research Center for Traditional Chinese Medicine, Key Laboratory of Chemical Biology and Molecular Engineering of Ministry of Education, Shanxi University, Taiyuan, 030006, China
[c] School of Ethnic-Minority Medicine, Guizhou Minzu University, Guiyang, 550025, China

ARTICLE INFO

Article history:
Received 23 February 2024
Received in revised form
5 July 2024
Accepted 9 July 2024
Available online 14 July 2024

Keywords:
Ulcerative colitis
Phillygenin
TGR5
Intestinal fibrosis
PERK-eIF2α-Ca^{2+} pathway

ABSTRACT

Ulcerative colitis (UC) is an idiopathic, relapsing, and etiologically complicated chronic inflammatory bowel disease. Despite substantial progress in the management of UC, the outcomes of mucosal barrier repair are unsatisfactory. In this study, phillygenin (PHI) treatment alleviated the symptoms of chronic colitis in mice, including body weight loss, severe disease activity index scores, colon shortening, splenomegaly, oxidative stress, and inflammatory response. In particular, PHI treatment ameliorated the tight junction proteins (TJs) reduction, fibrosis, apoptosis, and intestinal stem cell activity, indicating that PHI exerted beneficial effects on the intestinal mucosal barrier in mice with chronic colitis. In the NCM460 cells damage model, dextran sulfate sodium triggered the sequential induction of TJs reduction, fibrosis, and apoptosis. Takeda G protein-coupled receptor-5 (TGR5) dysfunction mediated NCM460 cell injury. Moreover, PHI treatment enhanced TJs and suppressed fibrosis and apoptosis to maintain NCM460 cell function, depending on TGR5 activation. PHI promoted TGR5 activation and elevated intracellular cyclic adenosine monophosphate levels in HEK 293T cells transfected with TGR5 expression plasmids. Cellular thermal shift assay and molecular docking studies confirmed that PHI directly binds to TGR5, indicating that PHI is an agonist of TGR5. The process of PERK-eIF2α pathway-mediated endoplasmic reticulum Ca^{2+} release was involved in NCM460 cell injury as well, which was associated with TGR5 dysfunction. When NCM460 cells were pretreated with PHI, the PERK-eIF2α pathway and elevated Ca^{2+} levels were blocked. In conclusion, our study demonstrated a novel mechanism that PHI inhibited the PERK-eIF2α-Ca^{2+} pathway through TGR5 activation to against DSS-induced TJs reduction, fibrosis, and apoptosis.

1. Introduction

Ulcerative colitis (UC), which is characterized by severe diarrhea, unexpected weight loss, bloody stools, abdominal pain, and fatigue, is a chronic relapsing-remitting inflammatory gastrointestinal disease, caused by impaired intestinal barrier function [1]. The intestinal epithelium is mainly formed by a tight continuous monolayer of intestinal epithelial cells (IECs), supported by tight junction proteins (TJs), which act as physical barriers to maintain mucosal homeostasis [2]. Destruction of TJs, mainly the zonula occludens-1 (ZO-1), E-cadherin, and occludin, can increase intestinal permeability, leading to systemic endotoxemia and inflammation [3]. Restoration of the intestinal mucosal tissue architecture is the standard outcome if inflammation is transient and mild. When inflammation persists in UC, the severity of damage to the intestinal barrier may exceed the intrinsic regenerative capacity of the affected tissue. The intestinal mucosa defends itself by developing a fibrotic response [4]. Epithelial-mesenchymal transition (EMT) is a pivotal intestinal fibrosis process, where specialized IECs populations give rise to myofibroblasts with fibrotic and pro-inflammatory activities [5]. Transition to mesenchymal phenotype involves the formation of spindle-shaped myofibroblasts, which express fibrotic marker, α-smooth muscle actin (α-SMA), but do not

* Corresponding author.
** Corresponding author.
E-mail addresses: lisf@sxu.edu.cn (S. Li), lwzhang@sxu.edu.cn (L. Zhang).

https://doi.org/10.1016/j.jpha.2024.101042

express the epithelial marker, occludin [6]. Intestinal fibrosis is thought to be an abnormal healing process, and the excessive production of extracellular matrix is ultimately responsible for increased tissue stiffness and progressive organ dysfunction [7]. Apoptosis is considered an anti-inflammatory cell death modality in most tissues, which alleviates fibrosis to some extent [8]. However, excessive apoptosis in IECs can promote the loss of barrier integrity, which may lead to microbes crossing the lumen into the lamina propria, inducing an excessive immune response and aggravating the pathological process of UC [9].

Currently, UC treatment primarily relies on controlling inflammatory and immunosuppressive mechanisms, which cannot completely treat UC and can lead to its recurrence [10]. Hence, in the treatment of UC, in addition to resisting inflammation, repairing the compromised intestinal mucosa is crucial. Above all, TJs reduction, fibrosis, and apoptosis in IECs are decisive factors in the destruction of the intestinal mucosal barrier, and multifaceted mechanisms need to be investigated.

Takeda G protein-coupled receptor-5 (TGR5), a transmembrane G protein-coupled bile acid receptor, is crucial for the regulation of metabolic disorders, such as obesity, inflammation, and glucose homeostasis [11]. TGR5 is ubiquitously expressed in various tissues, such as the gallbladder, brown adipose tissue, and entire gastrointestinal tract [12]. Recently, TGR5 has been shown to play a crucial role in intestinal barrier homeostasis. TGR5 can repair abnormal TJs structure [13], protect against IECs apoptosis [14], and promote intestinal stem cells (ISCs) renewal and regeneration [15]. However, the effect of TGR5 activation on UC-related intestinal fibrosis has not yet been elucidated. And the regulatory machinery of TGR5 in the pathological processes of TJs reduction, fibrosis, and apoptosis in IECs warrants further exploration.

Excessive endoplasmic reticulum stress (ERS) response in enterocytes is a hallmark of UC pathogenesis [16]. Moderate ERS maintains the balance of the intestinal environment, whereas severe ERS induces intestinal mucosal barrier dysfunction via the unfolded protein response (UPR) pathway [17]. The endoplasmic reticulum (ER) is an important organelle responsible for protein synthesis, transport, and Ca^{2+} regulation [18]. Severe ERS leads to Ca^{2+} release into the cytosol, resulting in various pathological alterations [19]. Elevated intracellular Ca^{2+} causes the TJs disruption and apoptosis in IECs, which can accelerate the pathological process of UC [20,21]. However, it is unclear whether TGR5 regulates the ERS-induced Ca^{2+} release, thereby participating in TJs reduction, fibrosis, and apoptosis.

Forsythia suspensa (Thunb.) Vahl (Oleaceae) was used to treat malignant ulcer, scrofula, carbuncle, gall tumor, rat fistula, heat, and poison in classical Chinese herbal texts [22]. Phillygenin (PHI) is a natural bioactive lignan derived from *Forsythia suspensa* that possesses the effects of anti-inflammatory, immune regulatory, and hepatoprotective effects [22]. PHI alleviated CCl_4-induced liver fibrosis, which is associated with regulation of the intestinal barrier [23]. Our previous study showed that PHI attenuated intestinal inflammation and enhanced TJs expression in the colon tissues of dextran sulfate sodium (DSS) induced acute colitis in mice [24]. However, the potential effects and mechanisms of action of PHI against chronic colitis and intestinal fibrosis in mice have not yet been explored. In present study, PHI maintained the intestinal mucosal barrier function, up-regulated TJs expression, and suppressed fibrosis and apoptosis in both DSS-induced chronic colitis mice and NCM460 cells. Mechanically, we revealed a new aspect of the underlying mechanism that PHI inhibited the PERK-eIF2α-Ca^{2+} pathway through TGR5 activation to defend against DSS-induced TJs reduction, fibrosis, and apoptosis.

2. Materials and methods

2.1. Materials and reagents

PHI (purity >98.0%) was extracted and purified from an ethanol extract of *Forsythia suspensa* leaves by our research group [25]. Kaempferol (B20527) was purchased from Yuanye Bio-Technology Co., Ltd (Shanghai, China). 5-Aminosalicylic acid (5-ASA; 89−57−6) was purchased from Aladdin Bio-Chem Technology Co., Ltd (Shanghai, China). The antibodies against matrix metallopeptidase 2 (MMP2; D261446) and eukaryotic translation initiation factor 2alpha (EIF2α; D163768) were purchased from Sangon Bioengineering Co., Ltd (Shanghai, China). The antibodies against ZO-1 (ab190085), E-cadherin (ab231303), occludin (ab216327), matrix metallopeptidase 9 (MMP9; ab76003), N-cadherin (ab76011), and p-EIF2α (ab32157) were purchased from Abcam (London, UK). Antibodies against collagen I (A1352), TGR5 (A20778), and yes-associated protein (YAP; A1002) were obtained from ABclonal Bio-technology Co., Ltd (Wuhan, China). The antibodies against α-SMA (GB111364−100) and cleaved caspase-3 (CY5501) were obtained from Servicebio Bio-technology Co., Ltd (Wuhan, China) and Abways Bio-technology Co., Ltd (Shanghai, China), respectively. The antibodies against protein kinase R-like endoplasmic reticulum kinase (PERK; CPA7063) and p-PERK (Phospho-T982) (CPA5833) were purchased from Cohesion Biosciences Co., Ltd (Shanghai, China).

2.2. Animals and treatments

Seven-week-old male C57BL/6J mice (18−22 g) were obtained from the Vital River Laboratory Animal Technology Co., Ltd. (Beijing, China). All experiments were conducted according to the guidelines of the Ethics Regulations of Shanxi University (Approval number: SXULL2022018). All mice were fed standard laboratory chow and water ad libitum and allowed to acclimatize to our facility for one week before experiments started.

Chronic colitis was induced in mice using DSS as previously described [26]. The experimental procedure is illustrated in Fig. 1A. Briefly, DSS (MW 36,000−50,000; MP Biomedicals, Santa Ana, CA, USA) was dissolved in drinking water to a concentration of 1.7% (*w*/*v*). The first two cycles consisted of 1.7% DSS for 5 days, followed by drinking water for 14 days. The third cycle consisted of 1.7% DSS for 5 days. The first and last days of DSS treatment were designated as days 1 and 43, respectively. The DSS solutions were changed every 2 days. After one cycle of DSS, mice developed colitis and were randomly divided into five groups ($n = 8$). From days 13 to 43, the mice were daily treated with PHI (25, 50, and 100 mg/kg) or 5-ASA (100 mg/kg) during concomitant colitis induction. The dosage selection of PHI (25, 50, and 100 mg/kg) and 5-ASA (100 mg/kg) in mice with chronic colitis was based on the acute colitis mice in our previous study [24]. PHI and 5-ASA were dissolved in 0.5% sodium carboxymethyl fiber (CMC-Na) solution. The control (CON) and DSS groups were daily administered the same volume of CMC-Na solution. During DSS treatment, body weight loss, stool consistency, and bloody stool were assessed every 2 days as indicators of disease activity index (DAI). The DAI scoring criteria have been previously described [24].

At the end of the treatment, the mice were sacrificed, and whole blood samples were collected for routine blood examination using 3-part differential hematology analyzer (BC-2800vet, Mindray, Shenzhen, China). The colons were removed, followed by length records. The 1-cm segment from the distal colonic tissue was immediately fixed with 4% (*v*/*v*) paraformaldehyde, and embedded

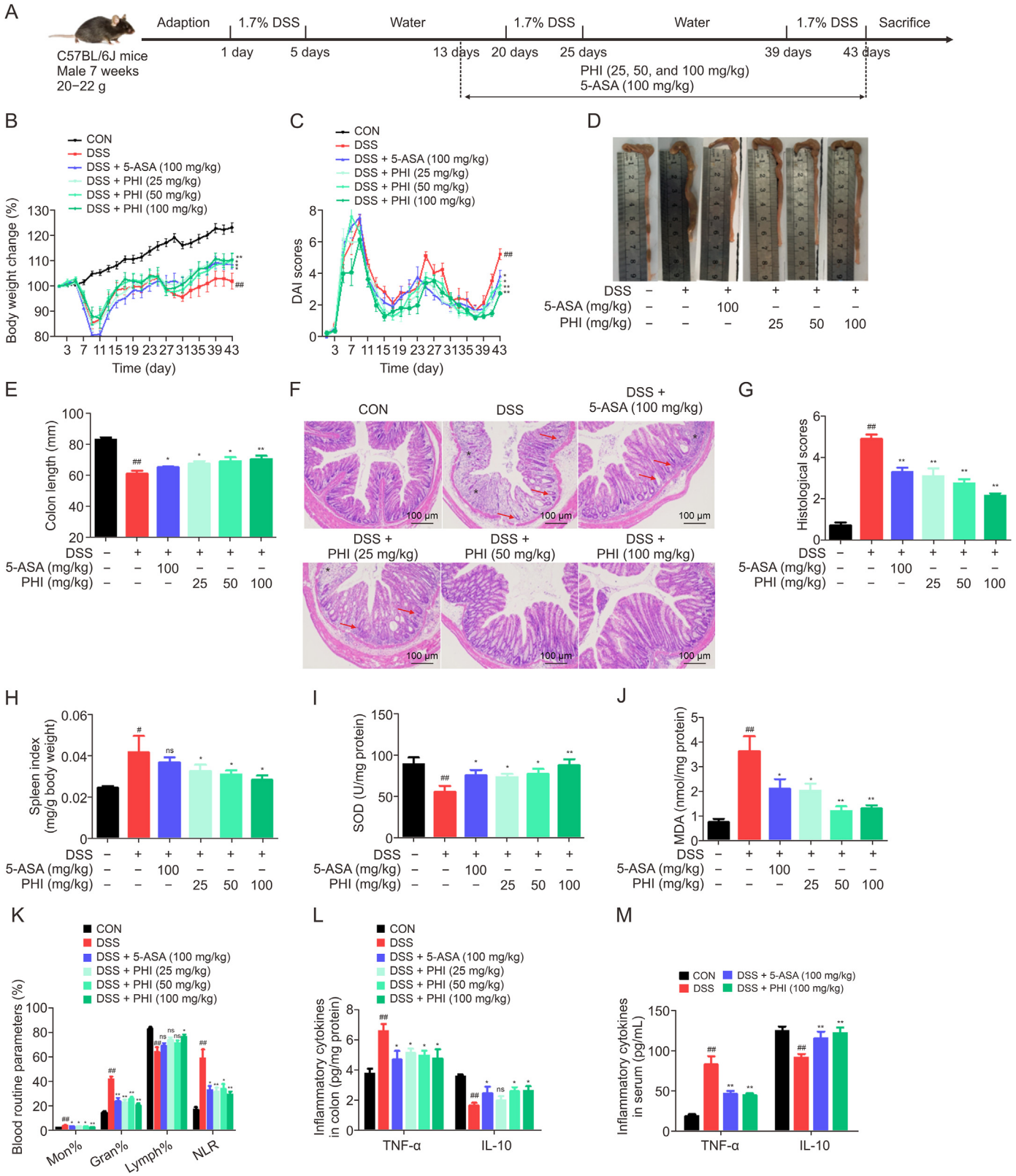

Fig. 1. Phillygenin (PHI) alleviated the symptoms in mice with chronic colitis. (A) Experimental design. (B, C) Body weight changes (B) and disease activity index (DAI) scores (C) from 1 to 43 days. (D, E) Representative photograph of colon (D) and colon lengths (E). (F) Representative colonic histological sections. Asterisks referred to inflammatory cell infiltration, while red arrows referred to goblet cells and crypts loss. (G) Colonic histological scores. (H) Spleen index. (I, J) The oxidative stress levels of superoxide dismutase (SOD) (I) and malondialdehyde (MDA) in colon tissues. (K) Routine blood examination of monocyte% (Mon%), granulocyte% (Gran%), lymphocyte% (Lymph%), and neutrophil-to-lymphocyte ratio (NLR) index. (L) The inflammatory cytokines of tumor necrosis factor-alpha (TNF-α) and interleukin-10 (IL-10) in colon tissues. (M) The inflammatory cytokines of TNF-α and IL-10 in serum. $^{\#\#}P < 0.01$ and $^{\#}P < 0.05$ vs. CON group; $^{**}P < 0.01$, and $^{*}P < 0.05$ vs. DSS group; ns: not significant. ($n = 6$–8 mice per group). CON: control; DSS: dextran sulfate sodium; 5-ASA: 5-aminosalicylic acid.

in paraffin. The sections were stained with hematoxylin and eosin. Histological injury of colon tissues was assessed by a combined score according to the previous method [27]. The spleen of mice was weighed and the spleen index was calculated. Superoxide dismutase (SOD) and malondialdehyde (MDA) levels in colon tissues were measured using commercially available kits (Jiancheng, Nanjing, China). Inflammatory cytokines, tumor necrosis factor-alpha (TNF-α) and interleukin-10 (IL-10), in colon tissues and serum were determined using enzyme-linked immunosorbent assay (ELISA) kits according to the manufacturer's instructions (Boster, Wuhan, China).

2.3. Terminal deoxynucleotidyl transferase-mediated dUTP nick end labeling (TUNEL) assay

A TUNEL Apoptosis Assay Kit (Servicebio Bio-technology Co., Ltd) was used to assess cell apoptosis according to the manufacturer's instructions. Three random fields were photographed from each section, and the average number of TUNEL-positive cells per field was calculated.

2.4. Masson trichrome staining

Masson trichrome staining was performed on paraffin-embedded colon tissues using reagents from Servicebio Bio-technology Co., Ltd, according to a standard procedure.

2.5. Real-time quantitative reverse transcription polymerase chain reaction (RT-qPCR)

The RNA was extracted from colon tissues using TRIzol reagent and reverse-transcribed into complementary cDNA using MightyScript Plus First Strand cDNA Synthesis Master Mix (Sangon, Wuhan, China). RT-qPCR was performed using the CFX96 PCR System (BIO-RAD, Hercules, CA, USA) with SYBR green mix. The mouse primer sequences are listed in Table S1.

2.6. Immunohistochemical staining

Colonic tissue sections were dewaxed, rehydrated, and repaired. Then, the sections were blocked for 30 min using 5% bovine serum albumin (BSA) and incubated overnight with primary antibodies against Ki67 (dilution 1:200), α-SMA (dilution 1:200), and collagen I (dilution 1:300) at 4 °C. Sections were incubated with an anti-rabbit IgG antibody at 25 °C for 30 min. Tissues were stained with the chromogen, diaminobenzidine. Images were acquired using an E100 light microscope (Nikon, Tokyo, Japan).

2.7. Metabolomics analysis

Colonic content samples were collected from the CON, DSS, and DSS + PHI (100 mg/kg) groups. The contents and solvent (methanol:acetonitrile = 3:1) were homogenized at a 1:10 (*w/v*) ratio to extract the metabolites. The quality control (QC) samples were prepared from 10 μL of each test sample to check the stability and performance of the instrument. Thermo-Fisher Dionex UltiMate 3000 UHPLC-Q Exactive Orbitrap-MS and Xcalibur workstation (Thermo Fisher Scientific, Waltham, MA, USA) were used to acquire ultra-high performance liquid chromatography-tandem mass spectrometry (UHPLC-MS/MS) raw data. The chromatographic separation was performed using an Acquity UPLC HSS T3 column (Waters, Milford, MA, USA). The mobile phase consisted of solvent A: 0.1% formic acid in water (*v/v*) and solvent B: acetonitrile, which was programmed as follows: 0–1 min, 2%–35% B; 1–15 min, 35%–70% B; 15–16 min, 70% B; 16–27 min, 70%–98% B; 27–27.5 min, 98%–2% B; 27.5–31 min, 2% B. The flow rate was set at 0.2 mL/min, and the injection volume was 5 μL. Mass spectrometry conditions were analyzed under positive and negative ionization modes, and the scan mode was *m/z* 80–1200. Compound Discoverer 3.0 software (Thermo Fisher Scientific) was used to obtain the matched peak data. SIMCA-P 14.1 software (Umetrics, Malmo, Sweden) was used for the multivariable statistics of the normalized data. Metabolites were identified using the online databases HMDB (http://www.hmdb.ca), ChemSpider (http://www.chemspider.com), and mzCloud (https://www.mzcloud.org/). Enrichment pathway analysis was performed using MetaboAnalyst (https://www.metaboanalyst.ca/).

2.8. 16S rRNA gene sequencing

The colonic contents were obtained from the CON, DSS, and DSS + PHI (100 mg/kg) groups, and frozen at −80 °C until use. Microbial DNA was isolated from colonic contents, and then V3–V4 region of the 16S rRNA of each sample was selected for amplification. The purified amplicons sequences were sequenced on an Illumina MiSeq platform (Illumina, San Diego, CA, USA). Data were analyzed by Majorbio Bio-Pharm Technology Co., Ltd (Shanghai, China).

2.9. Distribution of PHI in tissues/organs after single oral dose

PHI (100 mg/kg) was orally administered to C57BL/6J mice (n = 4 per time point). Serum, liver, colon tissue, and colonic contents (lumen contents within the colon tissues) were collected from wild-type (WT) mice at 0.5, 1, 2, 3, 4, and 8 h after PHI dosing. Using kaempferol as the internal standard, the PHI concentration was measured using an Acquity UPLC system (Waters). The mobile phase consisted of solvent A: acetonitrile, and solvent B: 0.1% formic acid in water (*v/v*), which was programmed as follows: 0–4 min, 5%–45% A; 4–15 min, 45%–50% A; 15–17 min, 50%–5% A. The flow rate was set at 0.2 mL/min, and the injection volume was 5 μL.

2.10. Cell cultures and treatments

Human colonic epithelial NCM460 cells were cultured in Dulbecco's modified Eagle medium supplemented with 100 U/mL penicillin, 100 μg/mL streptomycin, and 10% fetal bovine serum. For the DSS-stimulated NCM460 cell model, the cells were incubated with 2% DSS and harvested at 0, 3, 6, and 24 h time points. Control cells (Ctrl) were maintained in a medium containing phosphate buffered solution (PBS). For pretreatment, PHI (20 and 40 μM), 6α-ethyl-23(S)-methyl-3α,7α,12α-trihydroxy-5β-cholan-24-oic acid (INT-777, 20 μM; HY-15677, MCE, Merced, NJ, USA), m-tolyl 5-chloro-2-(ethylsulfonyl) pyrimidine-4-carboxylate (SBI-115, 100 μM; HY-111534, MCE), 2-aminoethyl diphenylborinate (2-APB; HY-W009724, MCE), 1,2-bis-(o-aminophenoxy)ethane-N,N,N',N'-tetra-acetic acid tetrakis(acetoxymethyl) ester (BAPTA-AM; HY-100545, MCE), and tauroursodeoxycholic acid (TUDCA; 14605–22–2, Yuanye, Shanghai, China) were added for 2 h before adding 2% DSS for 24 h.

2.11. Cellular viability analysis

The NCM460 cells were incubated with PHI for 24 h in 96-well plates. Cell viability was assessed using the Cell Counting Kit-8 assay following the manufacturer's instructions (Meilunbio, Dalian, China).

2.12. Fluorescein isothiocyanate (FITC)-dextran permeability assay

The NCM460 cells were seeded onto the apical side of Transwell chambers for 3 days to grow into dense monolayers. The cells were

pretreated with PHI (20 and 40 μM) for 2 h and exposed to 2% DSS for 24 h. Then, 1 mg/mL FITC-Dextran 4 kDa (FD-4) (Sigma, Saint Louis, MS, USA) was added to the apical side of the insets. After incubation for 2 h, the basolateral medium was collected, and the fluorescent intensity was measured using a SpectraMax iD5 microplate reader (Molecular Devices, Silicon Valley, CA, USA). Data are presented as percentages of the CON group.

2.13. Annexin V-FITC apoptosis assay

The NCM460 cells were cultured in 6-well plates at 37 °C in 5% CO_2. PHI was pretreated to the medium for 2 h, and then continuously stimulated with 2% DSS for 24 h. After washing with cold PBS and resuspending, the cells were stained with Annexin V-FITC and propidium iodide (PI) using an annexin V-FITC apoptosis detection kit (Meilunbio) according to the manufacturer's protocol. Fluorescence was measured using a CytoFlex flow cytometer (FCM, Beckman Coulter, Brea, CA, USA).

2.14. Measurement of calcium level

NCM460 cells were cultured in 6-well plates then exposed to 2% DSS for 1 h or 3 h. Control cells (Ctrl) were maintained in the medium containing PBS. For pretreatment, cells were pretreated with PHI (40 μM), INT-777 (20 μM), 2-APB (25 μM), BAPTA-AM (20 μM), and ethylene glycol tetraacetic acid (EGTA, 50 μM; HY-D0861, MCE) for 2 h, and then exposed in 2% DSS for 3 h to assess intracellular Ca^{2+} levels. Ca^{2+} marked by fluo-4 AM (Beyotime, Shanghai, China) was assessed using a CytoFlex FCM (Beckman Coulter, Brea, CA, USA). Green fluorescence of Ca^{2+} was visualized and photographed using an ortho-fluorescent microscope (Nikon).

2.15. Small-interfering RNA and transient transfection

The small interfering RNA (siRNA) targeting TGR5 was obtained from OBiO Technology Corp., Ltd. (Shanghai, China). The sequences of siTGR5 (siRNA TGR5) were as follows: sense: 5′-GUGUCGACCUGGACUUGAACUTT-3′ and antisense: 5′-AGUUCAAGUCCAGGUCGACACTT-3′. The sequences of siNC (siRNA negative control) were as follows: sense: 5′-UUCUCCGAACGUGUCACGUTT-3′ and antisense: 5′-ACGUGACACGUUCGGAGAATT-3′. The siTGR5 (100 nM) or siNC (100 nM) was transfected into NCM460 cells using the HighGene transfection reagent (RM09014, ABclonal Bio-technology Co., Ltd). After 12 h of incubation, the transfection medium was replaced with normal serum-free medium for 24 h to recover cell growth. After further treatment, the cells were harvested and subjected to Western blotting and immunofluorescence assays.

2.16. TGR5 luciferase assay

The effect of PHI on TGR5 activation was tested in HEK 293T cells as previously described [28]. The HEK 293T cells were transfected with the human TGR5 expression plasmid (100 ng) (MOD05005, APExBIO, Houston, TX, USA), CRE-driven luciferase reporter gene plasmid pGL4.29 (100 ng), and internal reference plasmid pRL-TK (100 ng) using Lipofectamine 3000 reagent (Thermo Fisher Scientific) for 12 h (Fig. S1). Then PHI (20 and 40 μM) or INT-777 (20 μM) was used to treat HEK 293T cells for 24 h. The cells were incubated with PBS as a vehicle. Cell lysates from different HEK 293T cell groups were analyzed using a dual-luciferase reporter gene assay kit (Beyotime, Shanghai, China) according to the manufacturer's protocol.

2.17. Cyclic adenosine monophosphate (cAMP) secretion measurement

Lysates from different HEK 293T cell groups were prepared as described for the TGR5 luciferase assay. Besides, PHI (20 and 40 μM) was added 2 h before adding 2% DSS to the NCM460 cells. NCM460 cell lysates were obtained after DSS stimulation for 3 h. The cAMP content was determined using an ELISA kit (Bioswamp, Wuhan, China).

2.18. Cellular thermal shift assay (CETSA)

NCM460 cells were incubated with PHI (40 μM) for 12 h. Cells were harvested and resuspended in PBS containing protease inhibitor. The cell suspensions were divided into six aliquots and heated at various temperatures, respectively. Heat-treated cell suspensions were frozen and thawed triple in liquid nitrogen. After centrifugation of the cell lysates, the supernatants were collected for Western blotting analysis.

2.19. Molecular docking

The crystal structure of human TGR5 was downloaded from the Protein Data Bank (PDB: 7BW0). PHI and TGR5 were combined using AutoDock. The protein structure was fixed during molecular docking. The functional binding pocket of the TGR5 crystal was used to investigate the PHI docking conformations, and their binding energies were calculated using the molecular mechanics Poisson Boltzmann surface area.

2.20. Immunofluorescence analysis

Paraffin sections of the colon tissue were prepared for immunohistochemical staining as previously described. NCM460 cells were treated with 4% (*v/v*) paraformaldehyde and fixed for 30 min. Colon sections and NCM460 cells were blocked with 5% (*w/v*) BSA for 30 min. Sections were incubated with primary antibodies against occludin (1:200), N-cadherin (1:200), and α-SMA (1:200) at 4 °C overnight, followed by incubation with a Cy3 goat anti-rabbit IgG secondary antibody for 10 min. Nuclei were counterstained with 4',6-diamidino-2-phenylindole (DAPI) for 10 min. The fluorescent images were obtained using an ortho-fluorescent microscope (Nikon).

2.21. Western blotting assay

Western blotting analysis was performed as previously described [24]. The optical density from the Western blotting assay was quantified using Image-Pro Plus software 6.0 (Media Cybernetics, Bethesda, MD, USA).

2.22. Statistical analysis

Data were analyzed using SPSS16.0. Two groups were compared using Student's *t*-test (two-tailed), whereas analysis of variance (ANOVA) was used to compare multiple groups. The value of $P < 0.05$ was considered statistically significant. All data were presented as mean ± standard error of the mean (SEM).

3. Results

3.1. PHI treatment alleviated the symptoms in mice with chronic colitis

Experimental chronic colitis was induced in mice by administering three cycles of 1.7% DSS in drinking water. During cyclic

stimulation with DSS, colitis mice exhibited self-healing abilities, as indicated by body weight loss, severe DAI scores, and colon shortening, followed by gradual recovery, which manifested symptoms similar to those of human UC (Figs. 1B–E). To investigate the therapeutic capacity of PHI in mice with chronic colitis, PHI (25, 50, and 100 mg/kg) or 5-ASA (100 mg/kg) was orally administered daily from day 13 to the end point. PHI treatment showed therapeutic effects in mice with chronic colitis in a dose-dependent manner, as evidenced by recovered body weight loss, lower DAI scores, and reduced colon shortening (Figs. 1B–E). Histologically, DSS induced severe goblet cell and crypt loss, dense inflammatory cell infiltration, and high histological scores; PHI treatment prevented these changes (Figs. 1F and G). Additionally, mice with chronic colitis exhibited an increased spleen index (Fig. 1H), which is generally related to the extent of inflammation and anemia [29]. PHI treatment mitigated the splenomegaly in mice with chronic colitis (Fig. 1H). Accompanied by repeated DSS exposure and severe bleeding, the mice with chronic colitis showed oxidative stress and inflammatory damage. Compared to those of control mice, lower SOD activity and higher MDA levels were observed in mice with chronic colitis, which were visibly reversed in the colon after PHI treatment (Figs. 1I and J). Furthermore, routine blood examination showed the PHI treatment ameliorated the monocyte% (Mon%), granulocyte% (Gran%), lymphocyte% (Lymph%) and neutrophil-to-lymphocyte ratio (NLR) in mice with chronic colitis (Fig. 1K). The NLR is considered an important parameter for assessing systemic inflammatory status and infection risk, indicating an inflammatory response in mice with chronic colitis [30]. PHI treatment also decreased the levels of colon and serum inflammatory cytokines, TNF-α and IL-10 (Figs. 1L and M). These results suggest that PHI played a potential therapeutic on DSS-induced chronic colitis mice.

3.2. PHI treatment maintained the intestinal mucosal barrier function through up-regulating TJs expressions and inhibiting IECs apoptosis

The intestinal epithelium functioning as a physiological construct maintains mucosal homeostasis and defends against

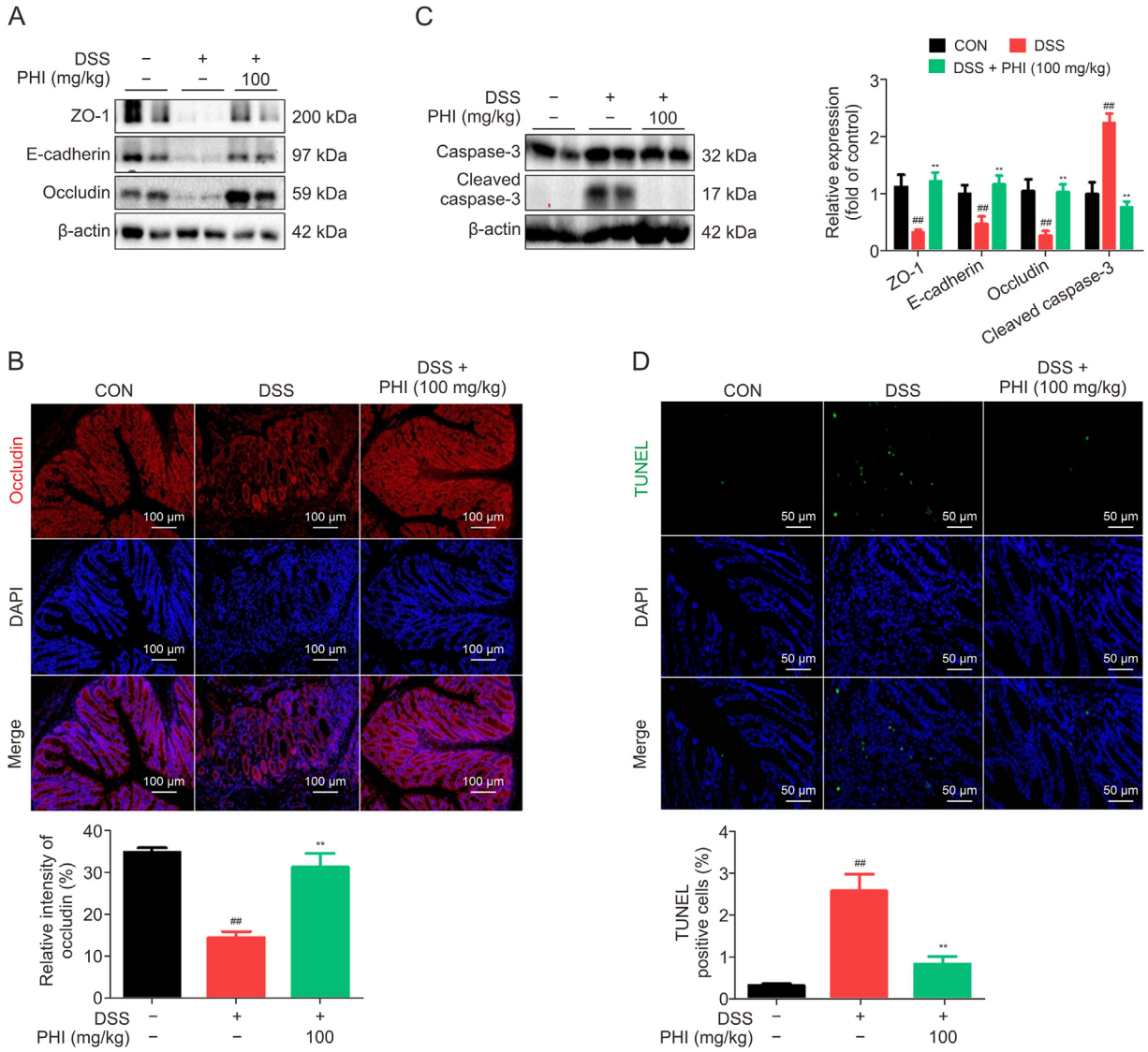

Fig. 2. Phillygenin (PHI) treatment enhanced the tight junction proteins (TJs) expressions and repressed the apoptosis of intestinal epithelial cells (IECs) in mice with chronic colitis. (A, C) Zonula occludens-1 (ZO-1), E-cadherin, occludin (A), cleaved caspase-3 and caspase-3 (C) were detected by Western blotting assay, and quantified bands by β-actin. (B) Representative colonic sections subjected to immunofluorescent staining with occludin and quantitation of fluorescence intensity. (D) Representative colonic sections subjected to terminal deoxynucleotidyl transferase-mediated dUTP nick end labeling (TUNEL) staining, and quantitation of TUNEL-positive cells. $^{\#\#}P < 0.01$ vs. CON group; $^{**}P < 0.01$ vs. DSS group. ($n = 3$–6 mice per group). CON: control; DSS: dextran sulfate sodium; DAPI: 4',6-diamidino-2-phenylindole.

exogenous antigens from bacteria, depending on TJs integrity [31]. In contrast to control mice, the mice with chronic colitis exhibited a reduction in TJs (ZO-1, E-cadherin, and occludin), whereas PHI up-regulated TJs expression (Fig. 2A). Consistently, disruption was observed in mice with chronic colitis by fluorescent staining with occludin, and the restorative effect of PHI on occludin was further confirmed (Fig. 2B). Excessive apoptosis of IECs leads to destruction of the intestinal mucosal barrier function. Mice with chronic colitis exhibited elevated levels of cleaved caspase-3 protein, which were remarkably reduced after PHI administration (Fig. 2C). In addition, TUNEL-positive cells were markedly increased in the colonic epithelium of mice with chronic colitis, and PHI treatment suppressed TUNEL-positive cells (Fig. 2D). These results suggest that PHI up-regulated TJs expression and reduced IECs apoptosis in mice with chronic colitis.

3.3. PHI treatment restrained the collagen depositions to attenuate intestinal fibrosis in mice with chronic colitis

UC-related intestinal fibrosis is a considerable complication that cannot be ignored, leading to the loss of colon tissue function and motility [32]. Fibrosis-associated mucosal collagen fibers deposition in the colonic tissue were visualized using Masson trichrome and immunohistochemistry staining (collagen I and α-SMA) in mice with chronic colitis, whereas PHI treatment clearly prevented the fibrosis (Figs. 3A–F). Western blotting results showed that fibrotic proteins of collagen I and α-SMA were increased in mice with chronic colitis, and PHI treatment reduced their expression, which was also confirmed through the RT-qPCR analysis of mRNA levels of *Col1a1* and *α-SMA* (Figs. 3G–I). Consistently, the fibrosis-related indicators of MMP2 and MMP9 exhibited higher protein expression in mice with chronic colitis, whereas PHI inhibited the MMP activity (Figs. 3G and H). Moreover, PHI treatment reduced the protein and mRNA levels of the elevated EMT marker, N-cadherin, in the colon tissues of mice with chronic colitis (Fig. 3G–I). These results demonstrate that PHI treatment restrained collagen deposition to attenuate intestinal fibrosis in mice with chronic colitis.

3.4. PHI treatment improved the ISCs proliferation and differentiation to regenerate the intestinal epithelium in mice with chronic colitis

In addition to the damage caused by TJs reduction, fibrosis, and apoptosis, the regenerative capacity of IECs must be tightly regulated to maintain intestinal homeostasis. Rapid renewal of the intestinal epithelium is sustained by ISCs, which terminally differentiate into different types of specialized IECs, such as absorptive (enterocytes) and secretory (Paneth cells and enteroendocrine cells) lineages [33]. The ISCs proliferation marker, Ki67, was already decreased and dispersed throughout the crypts in mice with chronic colitis rather than at the base of the crypts, where the proliferative cells should reside, as shown in control mice (Figs. 4A and B). PHI improved the distribution of Ki67 in the crypts,

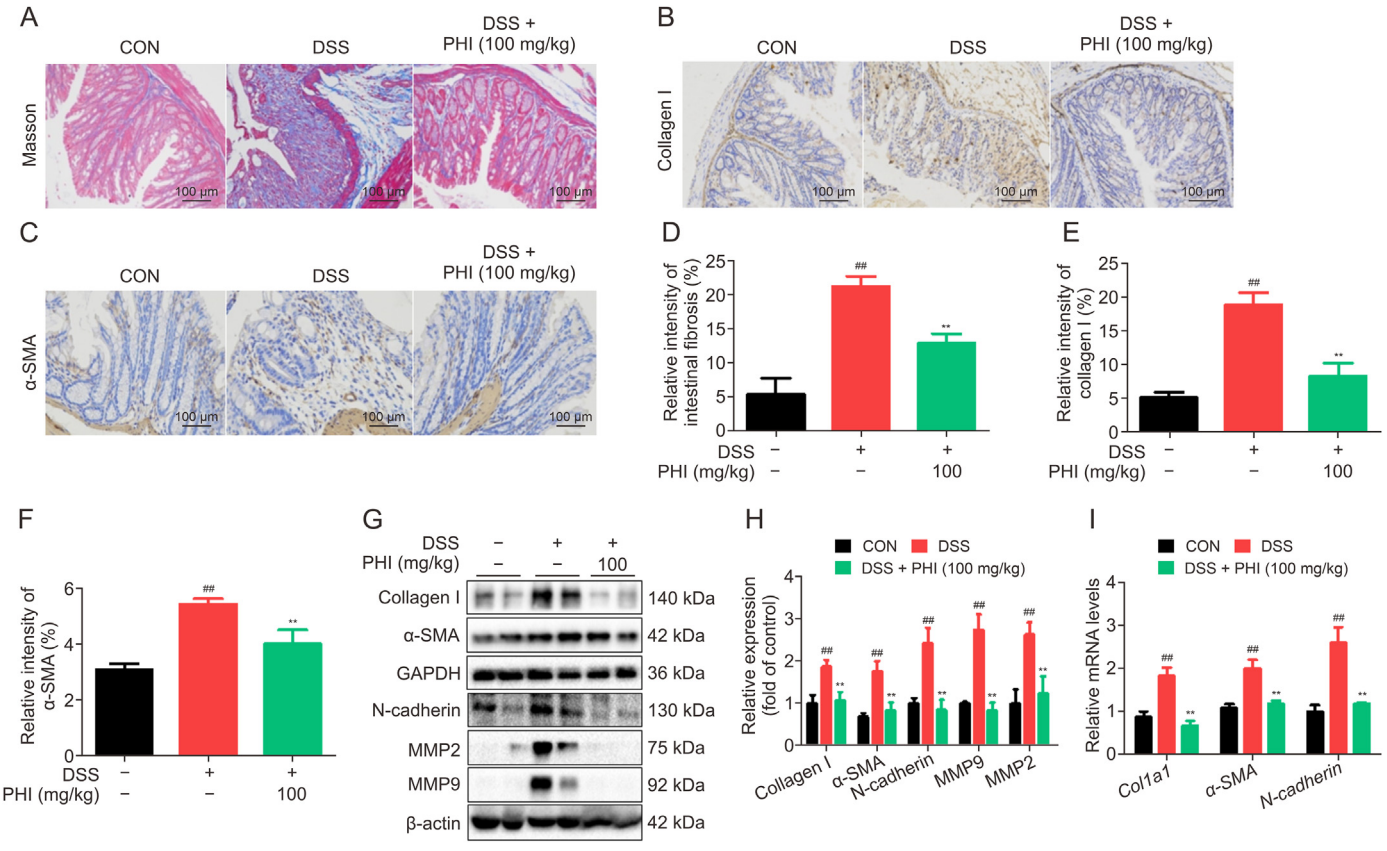

Fig. 3. Phillygenin (PHI) treatment attenuated intestinal fibrosis in mice with chronic colitis. (A) Representative images of Masson staining in colon tissues of mice with chronic colitis. (B, C) Immunohistochemical staining of collagen I (B) and α-smooth muscle actin (α-SMA) (C) of colon tissues. (D–F) Quantitation intensity of internal fibrosis (D), collagen I (E), and α-SMA (F), respectively. (G, H) Collagen I, α-SMA, N-cadherin, matrix metallopeptidase 2 (MMP2), and matrix metallopeptidase 9 (MMP9) were detected by Western blotting assay in mice with chronic colitis (G) and quantified bands by glyceraldehyde-3-phosphate dehydrogenase (GAPDH) or β-actin (H). (I) Real-time quantitative reverse transcription polymerase chain reaction (RT-qPCR) analysis of mRNA expression levels of *Col1a1*, *α-SMA*, and *N-cadherin*. $^{\#\#}P < 0.01$ vs. CON group; $^{**}P < 0.01$ vs. DSS group. ($n = 3$–6 mice per group). CON: control; DSS: dextran sulfate sodium.

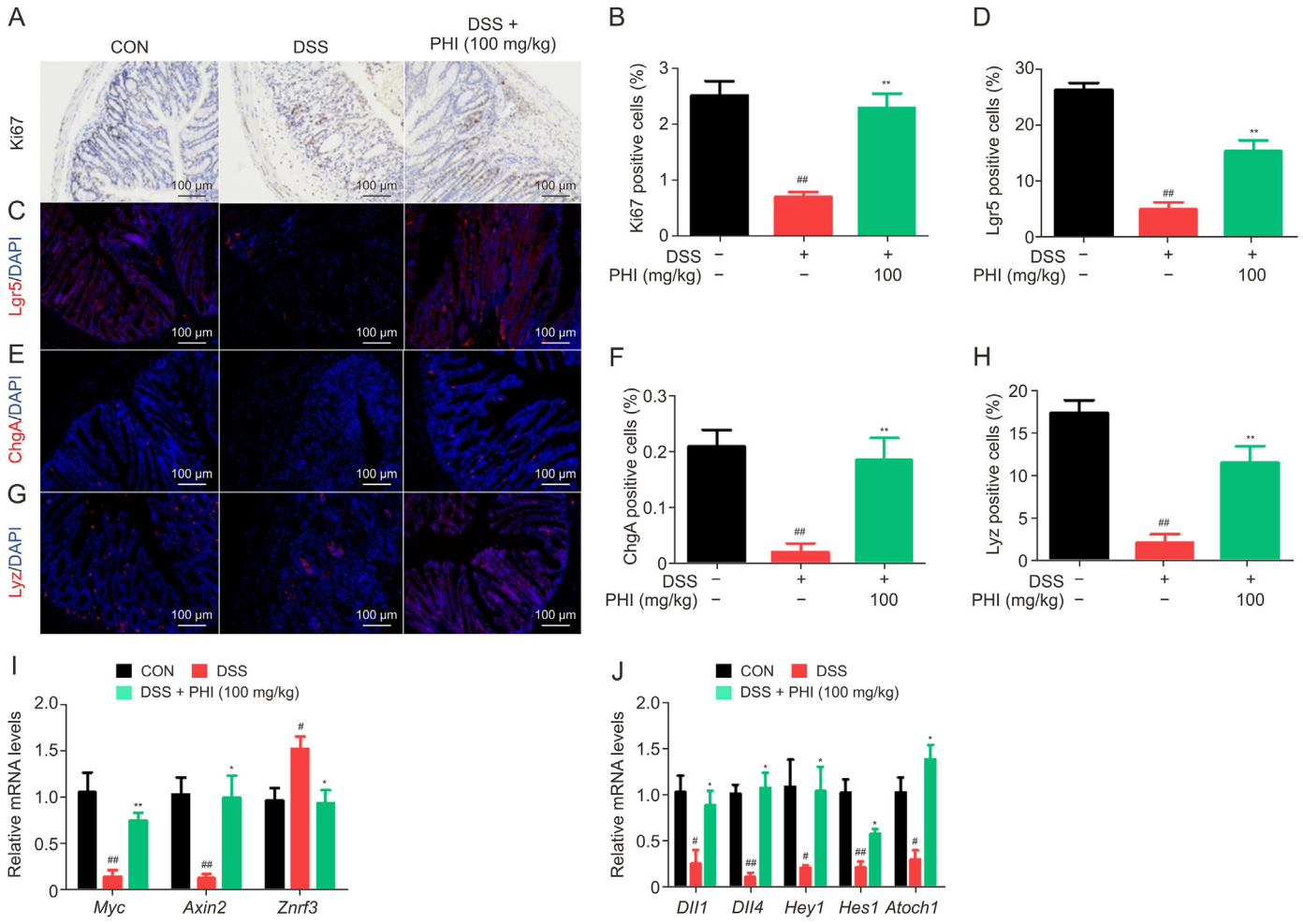

Fig. 4. Phillygenin (PHI) treatment improved the intestinal stem cells (ISCs) proliferation and differentiation in mice with chronic colitis by regulating Wnt and Notch signaling. (A, B) Colon cross section stained with Ki67 (A) and quantification of proliferation cells (B). (C–H) Immunofluorescence staining of leucine-rich repeat-containing G protein-coupled receptor 5 (Lgr5) (C), chromogranin A (ChgA) (E), and lysozyme (Lyz) (G) in the crypt, and quantification of Lgr5 (D), ChgA (F), and Lyz (H) positive cells intensity, respectively. (I, J) Real-time quantitative reverse transcription polymerase chain reaction (RT-qPCR) analysis of Wnt signaling genes (*Myc*, *Axin2*, and *Znrf3*) and Notch signaling genes (*Dll1*, *Dll4*, *Hey1*, *Hes1*, and *Atoch1*). $^{\#\#}P < 0.01$ and $^{\#}P < 0.05$ vs. CON group. $^{**}P < 0.01$, and $^{*}P < 0.05$ vs. DSS group. ($n = 3–6$ mice per group). CON: control; DSS: dextran sulfate sodium; DAPI: 4',6-diamidino-2-phenylindole.

indicating that the mice had more proliferative cells to regenerate the intestinal epithelium (Figs. 4A and B). Fluorescent staining showed that the ISCs marker (leucine-rich repeat-containing G protein-coupled receptor 5 (Lgr5)), enteroendocrine cell marker (chromogranin A (ChgA)), and paneth cell marker (lysozyme (Lyz)) were augmented in the colons of mice with chronic colitis after PHI intervention (Figs. 4C–H). Moreover, the activities of ISCs are largely governed by surrounding niche factors. Wnt signaling-related genes are crucial for ISCs proliferation [34]. *Myc* and *Axin2* were expressed at lower levels and *Znrf3* was expressed at higher level in the intestinal epithelium of mice with chronic colitis, and PHI treatment reversed these changes (Fig. 4I). Notch signaling-related genes are crucial determinants of ISCs differentiation [34]. PHI treatment markedly increased the expression of the genes involved in Notch signaling (*Dll1*, *Dll4*, *Hes1*, *Hey1*, and *Atoh1*), which were substantially repressed in mice with chronic colitis (Fig. 4J). Therefore, PHI treatment promoted the activation of Notch and Wnt signal transduction to regulate ISCs proliferation and differentiation, thereby replacing constant IECs loss.

3.5. Gut microbiota-secondary bile acid axis-mediated TGR5 activation exerted an indirect role in PHI-treated mice with chronic colitis

To further investigate the mechanism of PHI in the treatment of chronic colitis in mice, untargeted metabolomics was performed on the colonic contents to understand the underlying metabolic changes. Principal component analysis (PCA) score plots showed that the metabolic profiles in DSS + PHI (100 mg/kg) group were closer to those in the CON group, suggesting that metabolic disturbances improved after PHI treatment (Fig. 5A). The QC samples were collected, which indicated that the instrument was stable (Fig. 5A). Partial least squares-discriminant analysis (PLS-DA) and permutation tests demonstrated that the model was reliable (Figs. S2A and B). Meanwhile, the orthogonal partial least squares-discriminant analysis (OPLS-DA) model was utilized to obtain variable importance for projection (VIP) values (Fig. S2C). Metabolites with substantial differences between the CON and DSS groups were screened according to VIP >1.0, S-plot,

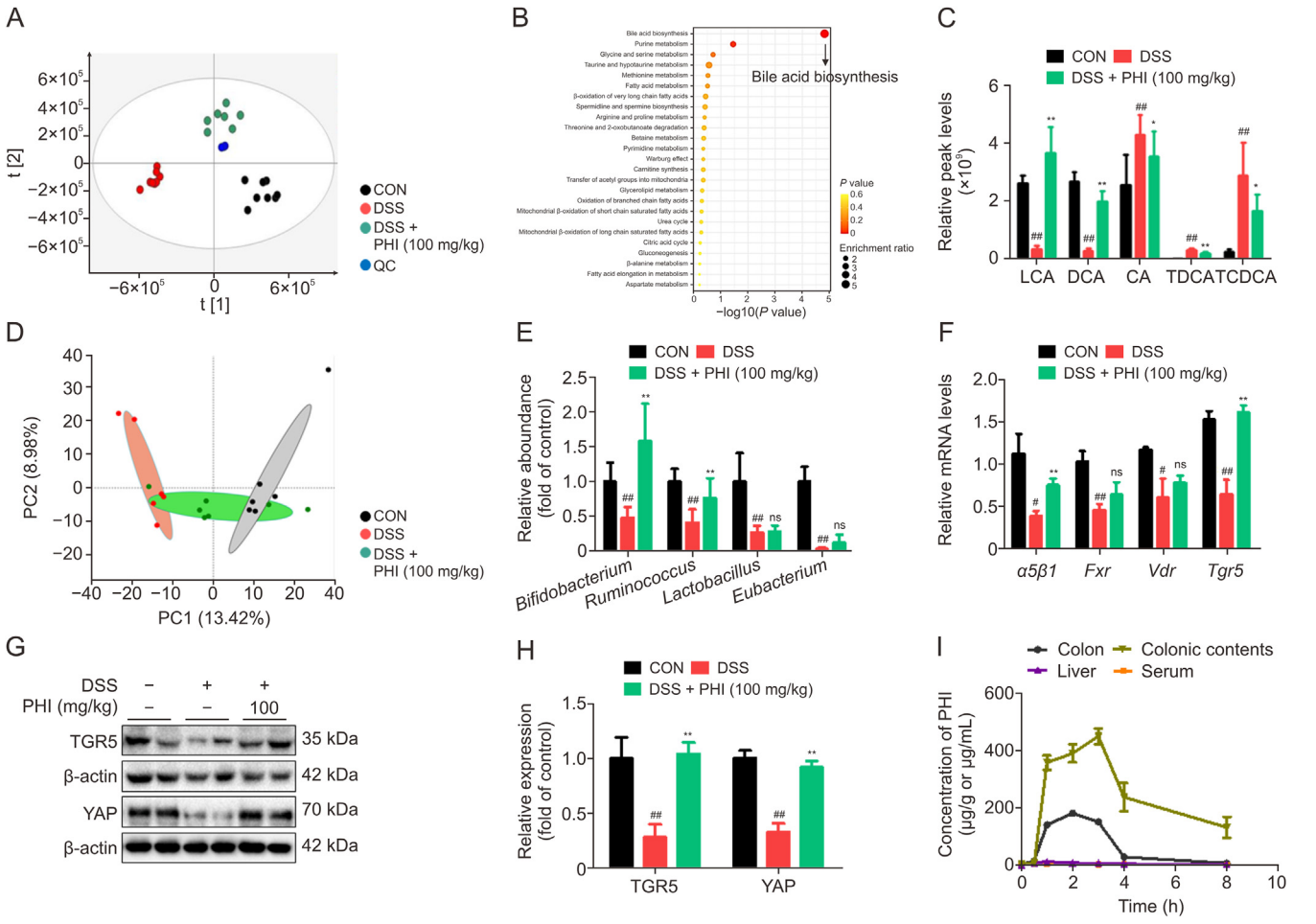

Fig. 5. Gut microbiota exerted an indirect role in secondary bile acids (BAs)-mediated Takeda G protein-coupled receptor-5 (TGR5) activation in phillygenin (PHI)-treated mice with chronic colitis. (A) Principal component analysis (PCA) score plots of metabolic profiling among the control (CON), dextran sulfate sodium (DSS), DSS + PHI (100 mg/kg) groups ($n = 8$). (B) Pathway enrichment analysis of 34 key differential metabolites using MetaboAnalyst 5.0. (C) The relative levels of lithocholic acid (LCA), deoxycholic acid (DCA), cholic acid (CA), tauroursodeoxycholic acid (TDCA), and taurochenodeoxycholic acid (TCDCA). (D) PCA score plots of microbial communities among CON, DSS, and DSS + PHI (100 mg/kg) groups at operational taxonomic unit (OTU) levels ($n = 6$). (E) The relative abundances of *Bifidobacterium*, *Ruminococcus*, *Lactobacillus*, and *Eubacterium* bacteria at genus levels. (F) Real-time quantitative reverse transcription polymerase chain reaction (RT-qPCR) analysis of mRNA expression levels of *α5β1*, *Fxr*, *Vdr*, and *Tgr5* ($n = 3$). (G, H) TGR5 and yes-associated protein (YAP) were detected by Western blotting assay in mice with chronic colitis (G), and quantified bands by β-actin (H) ($n = 6$). (I) The drug-time curve of PHI in the serum, liver, colon tissues, and colonic contents in wild-type (WT) mice ($n = 4$). $^{\#\#}P < 0.01$ and $^{\#}P < 0.05$ vs. CON group; $^{*}P < 0.05$ and $^{**}P < 0.01$ vs. DSS group; ns: not significant. QC: quality control.

and *t*-test ($P < 0.05$) (Figs. S2C and D). PHI treatment remarkably recovered 34 metabolites, as determined by cluster heatmap analysis (Fig. S2E). Pathway enrichment analysis of the 34 metabolites revealed that PHI mainly regulated the bile acid (BA) biosynthesis pathway (Fig. 5B). BA metabolic profiles showed higher levels of cholic acid (CA), tauroursodeoxycholic acid (TDCA), and taurochenodeoxycholic acid (TCDCA), and lower levels of lithocholic acid (LCA) and deoxycholic acid (DCA) in mice with chronic colitis (Fig. 5C), which was consistent with the disrupted BA metabolism in patients with UC [35]. PHI treatment improved the disrupted BAs (Fig. 5C).

Considering the role of gut microbiota-mediated BA metabolism, 16S rRNA sequencing of the colonic contents was performed. PCA showed that the flora profiles in the DSS + PHI (100 mg/kg) group were similar to those in the CON group, illustrating that PHI treatment partially recovered gut microbiota disturbances (Fig. 5D). We further analyzed the changes in the gut microbiota that mediate BA metabolism. BSH-producing bacteria, including *Bifidobacterium* and *Lactobacillus*, convert conjugated BAs into free BAs [36]. Meanwhile, *Ruminococcus* and *Eubacterium* that encode *bai* genes, can accomplish BA 7α-dehydroxylation process, ultimately leading to formation of the DCA from CA, and LCA from CDCA [37]. The results showed that *Bifidobacterium*, *Lactobacillus*, *Ruminococcus*, and *Eubacterium* bacteria were reduced in mice with chronic colitis, whereas PHI treatment upregulated the abundance of *Bifidobacterium* and *Ruminococcus* bacteria, but not *Lactobacillus* and *Eubacterium* bacteria (Fig. 5E). Thus, PHI treatment enhanced the *Bifidobacterium* abundance and reduced the levels of taurine-conjugated BA, including TDCA and TCDCA. The *Ruminococcus* abundance was enhanced by PHI treatment, thereby increasing the DCA and LCA levels and reducing the CA level. The secondary BAs (DCA and LCA) were reported to activate multiple receptors, mainly including the α5β1, farnesoid X receptor (FXR), vitamin D receptor (VDR), and TGR5 [38]. The results showed the mRNA expression levels of *α5β1*, *Fxr*, *Vdr*, and *Tgr5* in colon tissues were reduced in mice with chronic colitis (Fig. 5F). Among them, TGR5 was found to be the BA receptor with the best improvement after PHI supplementation (Fig. 5F). PHI treatment also enhanced the protein expression of TGR5 and its downstream YAP in mice with chronic colitis (Figs. 5G and H). Consequently, the therapeutic effects of PHI on mice with chronic colitis partially depend on *Bifidobacterium* and *Ruminococcus* bacteria mediate secondary BAs on TGR5 activation. TGR5 activation modulates the integrity of the intestinal mucosal

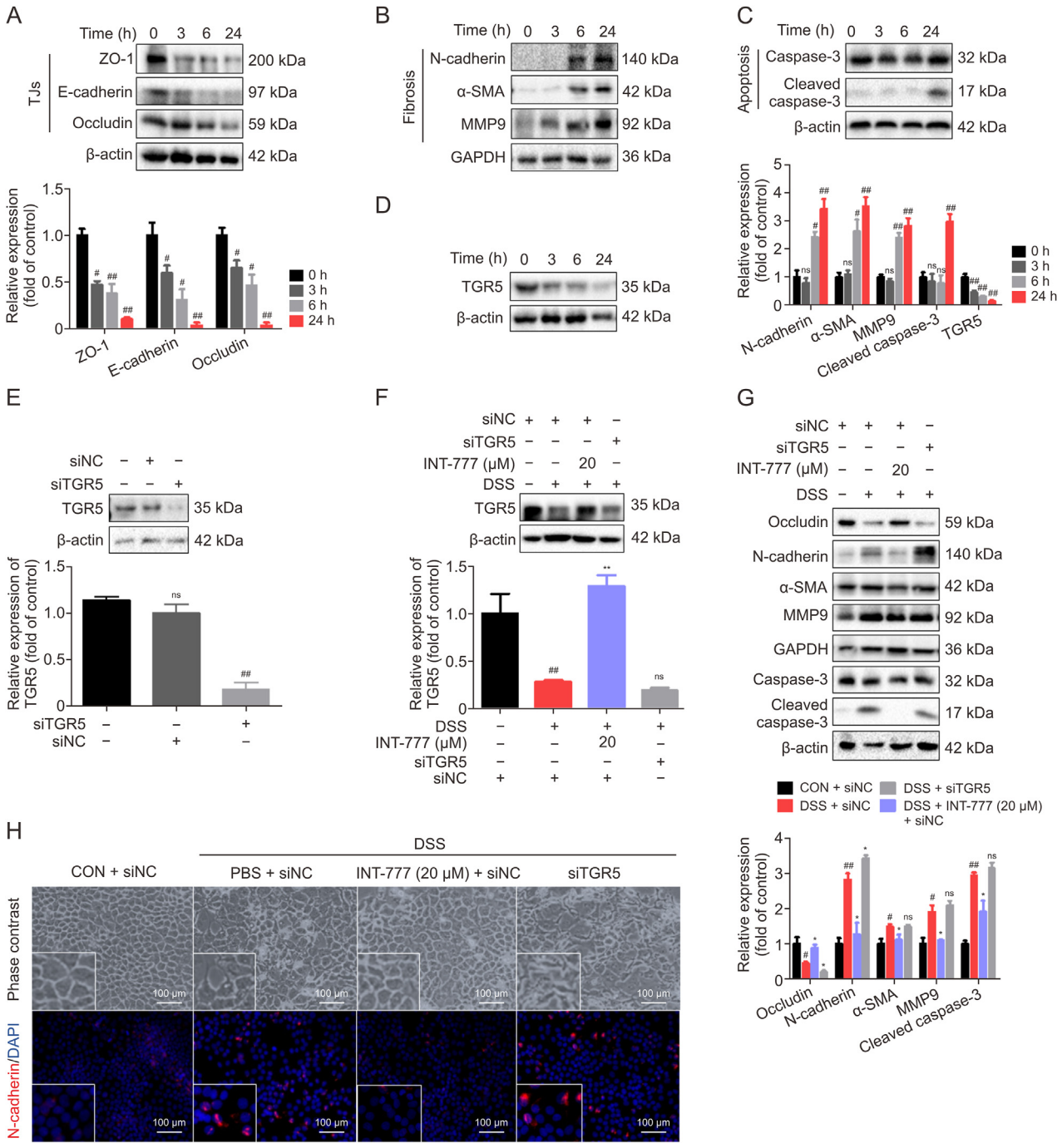

Fig. 6. Dextran sulfate sodium (DSS) triggered sequential induction of tight junction proteins (TJs) reduction, apoptosis, and fibrosis through disrupting Takeda G protein-coupled receptor-5 (TGR5) function in NCM460 cells. (A–D) NCM460 cells were treated with 2% DSS for various time (0, 3, 6, and 24 h). Cell lysates were analyzed for TJs (ZO-1, E-cadherin, and occludin) (A), fibrosis (N-cadherin, α-smooth muscle actin (α-SMA), and matrix metallopeptidase 9 (MMP9)) (B), apoptosis (cleaved caspase-3 and caspase-3) (C), and TGR5 (D) proteins by Western blotting assay, and quantified bands by β-actin or 4',6-diamidino-2-phenylindole (GAPDH). (E–H) NCM460 cells transfected with siRNA TGR5 (siTGR5) or siRNA negative control (siNC) before 36 h or pretreated with 6α-ethyl-23(S)-methyl-3α,7α,12α-trihydroxy-5β-cholan-24-oic acid (INT-777) (20 μM) for 2 h, and followed by 2% DSS stimulation for 24 h. The knockdown efficiency of siTGR5 was evaluated by Western blotting assay (E). TGR5, occludin, N-cadherin, α-SMA, MMP9, cleaved caspase-3, caspase-3 were detected by Western blot assay, and quantified bands by β-actin or glyceraldehyde-3-phosphate dehydrogenase (GAPDH) (F, G). (H) Representative images of phase contrast and immunofluorescence N-cadherin. $^{\#\#}P < 0.01$ and $^{\#}P < 0.05$ vs. Ctrl group; $^{**}P < 0.01$, and $^{*}P < 0.05$ vs. DSS group; ns: not significant. ($n = 3$). PBS: phosphate buffered solution; Ctrl: control cells; DAPI: 4',6-diamidino-2-phenylindole.

barrier [13–15]. However, the intestinal contents of DCA and LCA are typically low *in vivo*, and their effects on activation TGR5 are limited [39]. The results of the drug-time curve (Fig. 5I) and chromatogram (Fig. S3) indicated that the absorption of PHI in the serum and liver was quite low and mainly distributed in the colon tissues and colonic contents after oral administration. Hence, we speculated that PHI directly activated TGR5 in colon tissue, thereby prominently exerting the metabolic benefits of TGR5.

3.6. DSS triggered sequential induction of TJs reduction, fibrosis, and apoptosis through disrupting TGR5 function in NCM460 cells

First, we investigated whether the stimulation of NCM460 cells with 2% DSS *in vitro* induces TJs reduction, fibrosis, and apoptosis. The temporal relationships among TJs reduction, fibrosis, and apoptosis were assessed in DSS-induced NCM460 cells. The results showed that the expression of TJs (ZO-1, E-cadherin, and occludin) was disrupted after DSS exposure for 3 h, and continued to decrease until 24 h (Fig. 6A). Fibrosis markers (N-cadherin, α-SMA, and MMP9) appeared after DSS stimulation for 6 h, and continued fibration until 24 h (Fig. 6B). NCM460 cell apoptosis was detected only after DSS stimulation for 24 h, as indicated by the elevated levels of cleaved caspase-3 protein (Fig. 6C). These data suggest that DSS triggered the sequential induction of TJs reduction, fibrosis, and apoptosis in NCM460 cells. To further verify this pathological process, DSS-induced acute (7 days) and chronic (43 days) colitis were investigated. Immunofluorescence staining revealed the disruption of occludin in mice with both acute and chronic colitis (Figs. S4A and B). Masson trichrome staining results showed that although ulcerative damage was observed in the colons of mice with acute colitis, almost no collagen fibers were deposited (Figs. S4C and D). In contrast, excessive deposition of collagen fibers, a prominent feature of chronic colitis, was observed in the mucosal tissues of mice with chronic colitis (Figs. S4C and D). The number of colonic TUNEL-positive cells was also substantially higher in mice with chronic colitis than that in those with acute colitis (Figs. S4E and F). The *in vivo* results indicated that TJs reduction is a prerequisite for colitis, leading to continuous intestinal fibrosis and apoptosis. Furthermore, the expression of TGR5 was reduced after DSS stimulation for 3 h and continued to decrease until 24 h in NCM460 cells (Fig. 6D). To investigate whether DSS-induced NCM460 cell injury was mediated by TGR5 dysfunction, a TGR5-specific siRNA was used to suppress TGR5 expression (Fig. 6E). INT-777, a selective TGR5 agonist, rescued TGR5 loss in DSS-induced NCM460 cells, whereas siTGR5 treatment promoted TGR5 loss (Fig. 6F). INT-777 treatment also improved the reduction of occludin and decreased the expression of N-cadherin, α-SMA, MMP9, and cleaved caspase-3 proteins in DSS-induced NCM460 cells (Fig. 6G). In contrast, siTGR5 exacerbated the NCM460 cell damage (Fig. 6G). Phase-contrast images revealed the transition of DSS-induced EMT in NCM460 cells from an epithelial shape to a typical spindle-like fibroblastic shape (Fig. 6H). INT-777 treatment ameliorated the aberrant phenotypes, whereas siTGR5 treatment aggravated fibrotic damage (Fig. 6H). The immunofluorescence results also showed that INT-777 markedly decreased the expression of fibrotic marker N-cadherin, whereas TGR5 silencing facilitated fibrotic expression (Fig. 6H). These results indicate that DSS triggered the sequential induction of TJs reduction, fibrosis, and apoptosis, whereas TGR5 dysfunction accelerated the progression of NCM460 cell injury.

3.7. PHI activated TGR5 to suppress TJs reduction, fibrosis, and apoptosis in NCM460 cells

Next, we assessed the effects of PHI on DSS-induced injury in NCM460 cells. PHI (0—40 μM) had no impact on NCM460 cell viabilities within 24 h (Fig. S5A). PHI treatment also enhanced the expression of ZO-1, E-cadherin, and occludin (Fig. 7A). Similarly, the increased permeability of FD-4 in NCM460 monolayers caused by DSS was reduced by PHI treatment (Fig. S5B). PHI also attenuated DSS-induced fibrosis markers (N-cadherin, α-SMA, and MMP9), and the apoptosis marker, cleaved caspase-3 (Figs. 7B and C). PHI treatment enhanced the expression of TGR5 and its downstream target, YAP, in DSS-induced NCM460 cells, which was consistent with the results obtained in mice with chronic colitis (Fig. 7D). To further evaluate the role of TGR5 activation in the ameliorative effects of PHI on DSS-induced cell injury, we inhibited TGR5 activation using the specific inhibitor, SBI-115. The inhibitory effects on N-cadherin, α-SMA, MMP9, and cleaved caspase-3 proteins by PHI was abolished by simultaneous treatment with SBI-115 in DSS-induced NCM460 cells (Fig. 7E). Consistently, the siTGR5-treated NCM460 cells further demonstrated the inhibitory effects of PHI on occludin disruption, fibrosis (N-cadherin, α-SMA, and MMP9), and apoptosis (cleaved caspase-3) proteins were disappeared (Fig. 7F). Phase-contrast images revealed that silencing of TGR5 blocked the recovery of the DSS-induced spindle-like fibroblastic shape in NCM460 cells by PHI (Fig. 7G). The immunofluorescence results showed that the improvement effects of PHI on occludin, N-cadherin, and α-SMA were prevented in siTGR5-treated NCM460 cells (Fig. 7G). FCM results also showed that TGR5 silencing reduced the inhibitory effects on DSS-induced NCM460 cell apoptosis by PHI (Figs. S5C and D).

HEK 293T cells were transfected with TGR5 expression plasmid to gain further insight into the role of PHI in TGR5 activation. PHI greatly promoted TGR5 activation (Fig. 7H) and elevated intracellular cAMP levels in HEK 293T cells (Fig. 7I). Similarly, DSS reduced cAMP levels at 3 h in NCM460 cells, whereas PHI rescued cAMP loss (Fig. S5E). CETSA was used to determine the interaction between PHI and TGR5. The results showed that incubation of PHI with NCM460 cells increased the thermostability of the TGR5 protein and retarded its heat-degradation effect on TGR5 (Fig. 7J). The molecular docking results showed that PHI formed four hydrogen bonds with the TGR5 reporter by interacting with LEU262, GLY260, GLY258, and THR261 (Fig. S5F). The binding energy was −5.41 kcal/mol. These results indicate that PHI can directly bind to TGR5. Therefore, PHI treatment prevented DSS-induced TJs reduction, fibrosis, and apoptosis via TGR5 activation in NCM460 cells.

3.8. PHI treatment maintained NCM460 cell function via TGR5 mediated PERK-eIF2α-Ca^{2+} pathway

Excessive ERS activates PERK-eIF2α UPR pathway, which is the hallmark of UC pathogenesis [16]. The signaling cascades of the PERK-eIF2α pathway were activated after DSS stimulation for 3 h and continued until 24 h (Fig. 8A). To examine whether ERS-induced PERK-eIF2α pathway critically contributed to DSS-induced cell injury, NCM460 cells were pretreated with TUDCA, a recognized ERS inhibitor. TUDCA treatment suppressed the signaling cascades of both p-PERK and p-eIF2α (Fig. 8B). TUDCA also increased the occludin expression, and reduced the expressions of N-cadherin, α-SMA, MMP9, and cleaved caspase-3 proteins (Fig. 8C). These data suggest that the PERK-eIF2α pathway is involved in DSS-induced TJs reduction, fibrosis, and apoptosis in NCM460 cells. We next investigated the role of the PERK-eIF2α pathway in TGR5 signaling. INT-777 effectively restrained the eIF2α phosphorylation level, whereas siTGR5 treatment further heightened its phosphorylation (Figs. S6A and B), indicating that TGR5 activation down-regulated the PERK-eIF2α pathway. Moreover, PHI treatment suppressed the p-PERK and p-eIF2α levels in DSS-induced NCM460 cells (Fig. 8D). The similar inhibitory effects of PHI on the PERK-eIF2α pathway were observed in mice with chronic colitis (Fig. 8E). We investigated whether the effects of PHI were mediated by TGR5 activation. The results depicted that the inhibitory effects of PHI on p-PERK and p-eIF2α were vanished in siTGR5-treated NCM460 cells (Fig. 8F). Thus, PHI treatment inhibited PERK-eIF2α pathway through TGR5 activation.

The ER is the primary storage site of intracellular Ca^{2+} storage and plays an essential role in maintaining Ca^{2+} homeostasis [18]. To observe the changes on intracellular Ca^{2+} levels in DSS-induced NCM460 cells, Ca^{2+} was marked with fluo-4 AM. DSS stimulation

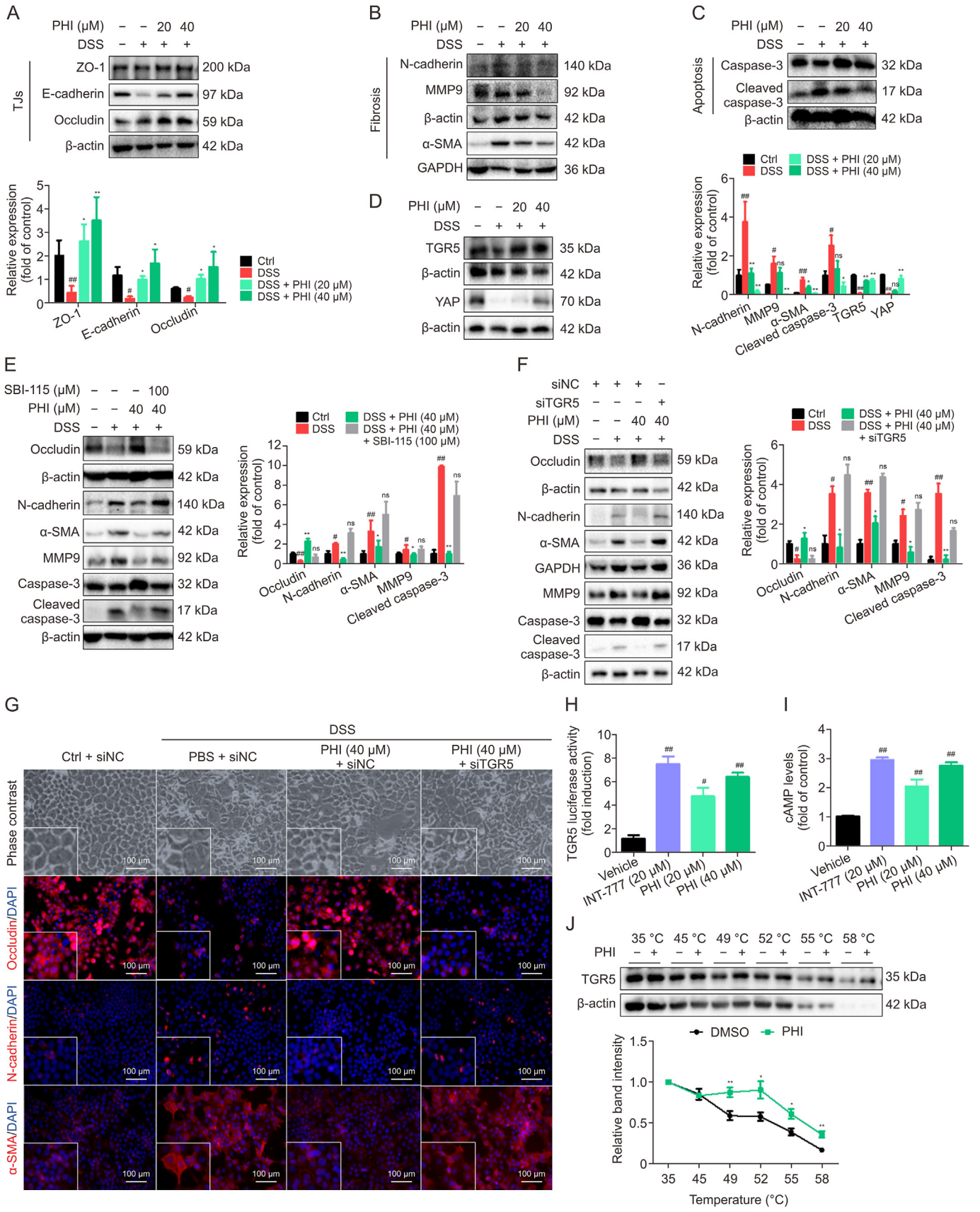

Fig. 7. Phillygenin (PHI) enhancing tight junction proteins (TJs), suppressing fibrosis and apoptosis to maintain NCM460 cell function through Takeda G protein-coupled receptor-5 (TGR5) activation. (A–D) NCM460 cells were pretreated with PHI (20 and 40 μM) for 2 h, and then treated with 2% dextran sulfate sodium (DSS) for 24 h. Zonula occludens-1 (ZO-1), E-cadherin, occludin (A), N-cadherin, á-smooth muscle actin (á-SMA), matrix metallopeptidase 9 (MMP9) (B), cleaved caspase-3, caspase-3 (C), TGR5, and yes-associated protein

resulted in a dramatic increase in intracellular Ca^{2+} at 3 h; however, no increase in Ca^{2+} levels was detected at 1 h (Fig. 9A). To study whether the elevated intracellular Ca^{2+} originated from the ER, NCM460 cells were pretreated with the IP3R inhibitor 2-APB or extracellular Ca^{2+} chelating agent EGTA, which blocked ER Ca^{2+} release and extracellular Ca^{2+} entry, respectively. FCM analysis revealed that 2-APB treatment reduced basal Ca^{2+} levels, and EGTA failed to block Ca^{2+} at 3 h (Fig. 9B), indicating that DSS mainly caused ER Ca^{2+} release. 2-APB and the intracellular free Ca^{2+} chelator, BAPTA-AM, also protected NCM460 cells from DSS-induced occludin destruction, fibrosis (N-cadherin, α-SMA, and MMP9), and apoptosis (cleaved caspase-3) (Fig. 9C). TUDCA treatment inhibited the elevated intracellular Ca^{2+} levels in DSS-induced NCM460 cells (Fig. 9D). These findings suggest that the ERS-mediated PERK-eIF2α pathway induced Ca^{2+} release, thereby further promoting the progression of NCM460 cell injury. Further studies were conducted to investigate whether TGR5 activation regulates intracellular Ca^{2+}. FCM analysis and fluorescent probe imaging results showed that INT-777 treatment reduced intracellular Ca^{2+} levels, whereas TGR5 silencing further accelerated Ca^{2+} production at 3 h (Figs. 9E and S6C). Similarly, PHI treatment markedly reduced intracellular Ca^{2+} levels at 3 h, whereas the inhibitory effect of PHI on Ca^{2+} was eliminated after treatment with siTGR5 (Fig. 9F). Fluorescent probe images also confirmed that the inhibition of PHI on Ca^{2+} was vanished in siTGR5-treated NCM460 cells (Fig. 9G). These findings demonstrate that PHI alleviated TJs reduction, fibrosis, and apoptosis in DSS-stimulated NCM460 cells via the TGR5 mediated-PERK-eIF2α-Ca^{2+} signaling pathway.

4. Discussion

Disruption of the intestinal mucosal barrier is considered a crucial factor in the progression of UC. As the major component of intestinal mucosal tissues, IECs damage is a decisive event in UC, including TJs reduction, fibrosis, and excessive apoptosis [17]. PHI has been used to treat liver diseases; however, studies on intestinal diseases are relatively limited. By examining the tissue/organ distribution patterns, PHI was found to be mainly distributed in the colon tissues, which is of great importance in studying the therapeutic effect of PHI on UC and intestinal fibrosis. PHI treatment effectively alleviated TJs reduction, fibrosis, and apoptosis in DSS-induced chronic colitis and NCM460 cells. PHI treatment also facilitated intestinal epithelial regeneration in mice with chronic colitis by regulating ISCs proliferation and differentiation. Mechanistically, the effects of PHI on repairing the intestinal mucosal barrier are mainly achieved by activating the TGR5. Specifically, we investigated a novel mechanism by which PHI treatment inhibits the PERK-eIF2a-Ca^{2+} pathway through TGR5 activation to protect against DSS-induced TJs reduction, fibrosis, and apoptosis.

The roles of TGR5 in the regulation of energy expenditure, glucose metabolism, and bile acid metabolism have been well-established. TGR5 activation plays a critical role in the prevention of colitis, including TJs protection, ISCs regeneration, and the inhibition of IECs apoptosis [13–15]. In chronic kidney diseases, the activation of TGR5 attenuated renal fibrosis by inhibiting of oxidative stress and inflammation [40]. The 12α-hydroxylated BAs contribute to liver fibrosis via TGR5 activation [41], indicating that the TGR5 functions depend on the cell and tissue type. However, the effects of TGR5 activation on colitis-related intestinal fibrosis remain unclear. In this study, we established an *in vitro* intestinal epithelial damage model using DSS stimulation. The results showed that DSS triggered the sequential induction of TJs reduction, fibrosis, and apoptosis in NCM460 cells. The selective TGR5 agonist, INT-777, alleviated the DSS-induced spindle-shaped profibrotic phenotype in NCM460 cells. TJs reduction, fibrosis, and apoptosis induced by DSS were relieved by INT-777, whereas TGR5 dysfunction accelerated the progression of NCM460 cell injury. These results suggest that strategies that promote TGR5 activation can effectively prevent intestinal fibrosis. Furthermore, PHI maintained NCM460 cell function by up-regulating TJs expression, and suppressing fibrosis and apoptosis. PHI treatment also markedly up-regulated the protein expression of TGR5 in both DSS-induced chronic colitis and NCM460 cells. TGR5 silencing weakened the TJs protective, anti-fibrotic, and anti-apoptotic effects of PHI in NCM460 cells.

Considering the high level of PHI in colon tissues, we further ascertained whether PHI directly activated TGR5 to protect against intestinal barrier damage. Our results showed that PHI promoted TGR5 activation and elevated intracellular cAMP levels in HEK 293T cells transfected with TGR5 expression plasmid. PHI also rescued DSS-induced cAMP reduction in NCM460 cells. Functional activation of TGR5 promotes rapid intracellular cAMP production, leading to sequential downstream reactions that regulate various metabolic processes [42]. Hence, the rapid reduction in cAMP levels induced by DSS was attributed to TGR5 dysfunction. Furthermore, CETSA confirmed that PHI directly binds to TGR5. Molecular docking was also used to elucidate the stable binding posture of the TGR5 active sites with PHI, indicating that PHI is an agonist of TGR5. PHI treatment also up-regulated YAP expression in DSS-induced chronic colitis and NCM460 cells. YAP, a TGR5 downstream target protein, plays a central role in gut physiology, particularly during epithelial regeneration [43]. Thus, PHI may enhance NCM460 cell survival (Fig. S7) and intestinal epithelial regeneration in mice with chronic colitis via activation of the TGR5-YAP axis. Taken together, PHI maintained NCM460 cell function by enhancing TJs and suppressing fibrosis and apoptosis. These effects may be attributed to TGR5 activation.

We next explored the mechanism by which PHI-activated TGR5 prevent DSS-induced NCM460 cell injury. ERS contributes to various human diseases including inflammatory conditions, fibrosis, and metabolic disorders [44]. ERS has recently been implicated as a major contributor to the development and occurrence of UC [16]. A previous study suggested a critical role of the PERK-eIF2α UPR pathway in mediating the ERS-induced renal fibrosis [45]. PERK activation is initially protective and crucial for survival during, whereas prolonged PERK signaling can trigger pro-apoptotic signals [46]. Thus, the PERK-eIF2α pathway was predicted to be the vital event involved in TJs reduction, fibrosis and apoptosis. Our results indicated that DSS stimulation activated the PERK-eIF2α pathway from 3 h to 24 h in NCM460 cells, ultimately leading to cell apoptosis. The ERS inhibitor TUDCA

(YAP) (D) were detected by Western blotting assay, and quantified bands by β-actin or glyceraldehyde-3-phosphate dehydrogenase (GAPDH). (E) NCM460 cells were pretreated with m-tolyl 5-chloro-2-(ethylsulfonyl) pyrimidine-4-carboxylate (SBI- 115) (100 μM) for 2 h, and then treated with 2% DSS for 24 h, and occludin, N-cadherin, α-SMA, MMP9, cleaved caspase-3, caspase-3 were detected by Western blot assay, and quantified bands by β-actin. (F, G) NCM460 cells transfected with siRNA TGR5 (siTGR5) or siRNA negative control (siNC) before 36 h and then treated with PHI (40 ìM) for 2 h, and followed by 2% DSS stimulation for 24 h. Occludin, N-cadherin, á-SMA, MMP9, cleaved caspase-3, and caspase-3 were detected by Western blotting assay, and quantified bands by β-actin or GAPDH (F). Representative images of phase contrast and immunofluorescence analysis (occludin, N-cadherin, and α-SMA) (G). (H, I) The HEK 293T cells were transfected with human TGR5 expression plasmid, pGL4.29, and pRL-TK for 12 h, and then treated with PHI (20 and 40 μM) or INT-777 (20 μM) for 24 h. Relative luciferase activities were determined using dual luciferase reporter gene kit (H). Intracellular cyclic adenosine monophosphate (cAMP) levels were detected in NCM460 cell lysates using enzyme-linked immunosorbent assay kit (I). (J) The effect of PHI on thermal stability of the TGR5. $^{\#\#}P < 0.01$ and $^{\#}P < 0.05$ vs. Ctrl group; $^{**}P < 0.01$, and $^{*}P < 0.05$ vs.DSS group; ns: not significant. (n = 3). PBS: phosphate buffered solution; Ctrl: control cells; DAPI: 4',6-diamidino-2-phenylindole.

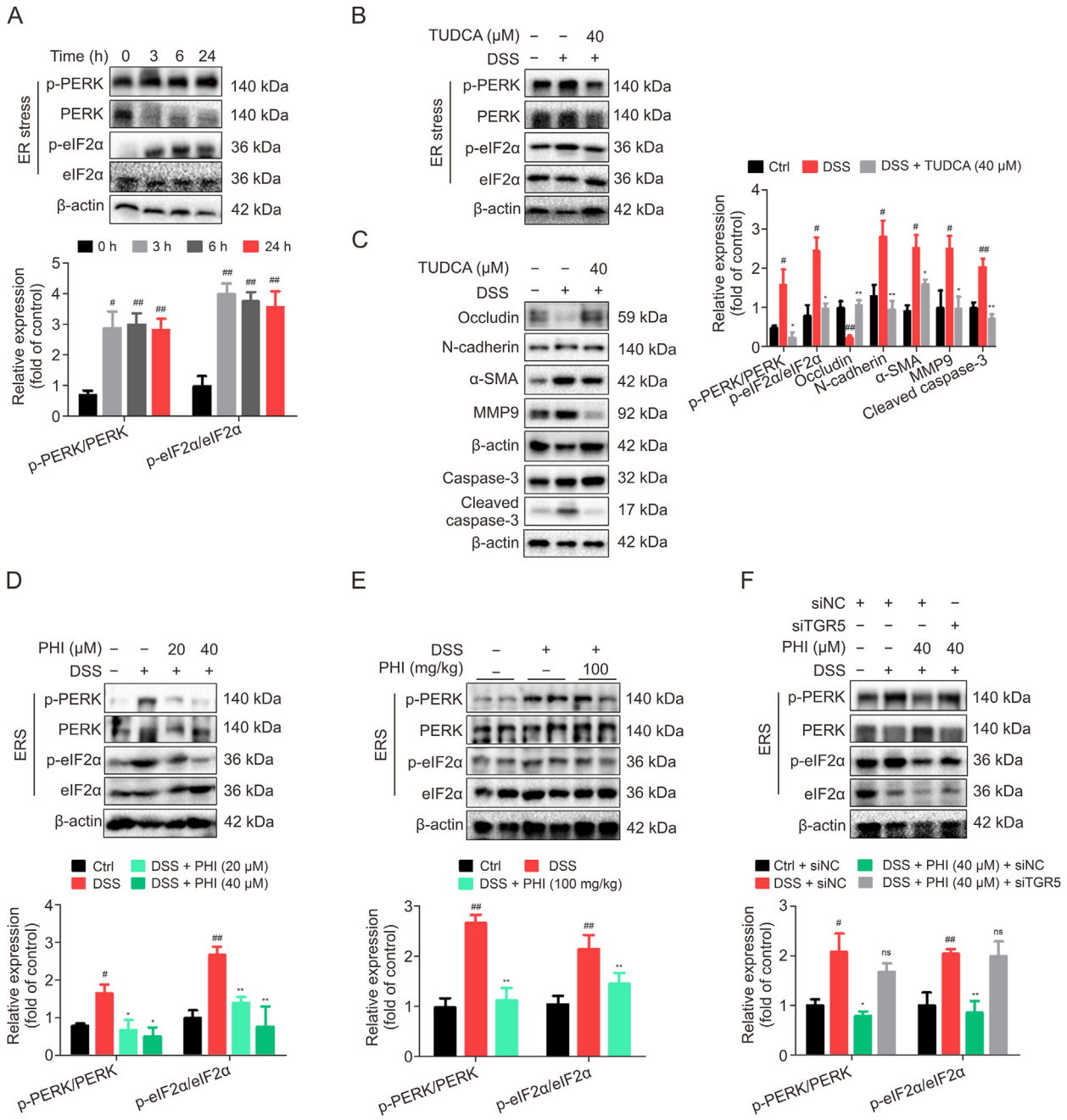

Fig. 8. Phillygenin (PHI) attenuated dextran sulfate sodium (DSS)-induced tight junction proteins (TJs) reduction, fibrosis, and apoptosis through the Takeda G protein-coupled receptor-5-protein kinase R-like endoplasmic reticulum kinaseeukaryotic translation initiation factor 2alpha (TGR5-PERK-eIF2α) pathway. (A) NCM460 cells were treated with 2% DSS for various time (0, 3, 6, and 24 h), and PERK/p-PERK, eIF2α/p-eIF2α were tested by Western blotting assay and quantified bands by β-actin. (B– D) NCM460 cells were pretreated with tauroursodeoxycholic acid (TUDCA) (40 μM) or PHI (20 and 40 μM) for 2 h, and followed by 2% DSS stimulation for 24 h. p-PERK/PERK, p-eIF2α/eIF2α, occludin, N-cadherin, α-smooth muscle actin (α-SMA), matrix metallopeptidase 9 (MMP9), cleaved caspase-3, caspase-3 were detected by Western blotting assay, and quantified bands by β-actin. (E) PERK/p-PERK, eIF2α/p-eIF2α were detected by Western blotting assay in mice with chronic colitis, and quantified bands by β- actin. (F) NCM460 cells transfected with siRNA TGR5 (siTGR5) or siRNA negative control (siNC) before 36 h were treated with PHI (40 μM) for 2 h and followed by 2% DSS stimulation for 24 h; then p-PERK/PERK, p-eIF2α/eIF2α were detected by Western blotting assay, and quantified bands by β-actin. $^{\#\#}P < 0.01$ and $^{\#}P < 0.05$ vs. Ctrl group; $^{**}P < 0.01$, and $^{*}P < 0.05$ vs. DSS group; ns: not significant. ($n = 3$). Ctrl: control cells; ERS: endoplasmic reticulum stress.

suppressed PERK-eIF2α pathway, and inhibited the TJs reduction, fibrosis, and apoptosis. These data indicate the critical role of the PERK-eIF2α pathway in DSS-induced NCM460 cell injury. Meanwhile, the TGR5 agonist, INT-777, down-regulated p-eIF2α expression in NCM460 cells, manifesting that TGR5 activation suppressed the PERK-eIF2α signaling. Similarly, PHI treatment restrained PERK-eIF2α signaling in both DSS-induced chronic colitis and NCM460 cells. When pretreated with siTGR5 in NCM460 cells, the inhibitory effect of PHI on PERK-eIF2α pathway disappeared. These results illustrate that PHI inhibit the PERK-eIF2α pathway in a TGR5 activation dependent manner.

Disruption of Ca^{2+} homeostasis is considered a key process in the pathogenesis of UC [47]. ERS leads to Ca^{2+} release, which facilitates the rapid transmission of Ca^{2+} signals and leads to distinctive biological outcomes [18]. Herein, DSS induced the dramatically higher intracellular Ca^{2+} levels in NCM460 cells,

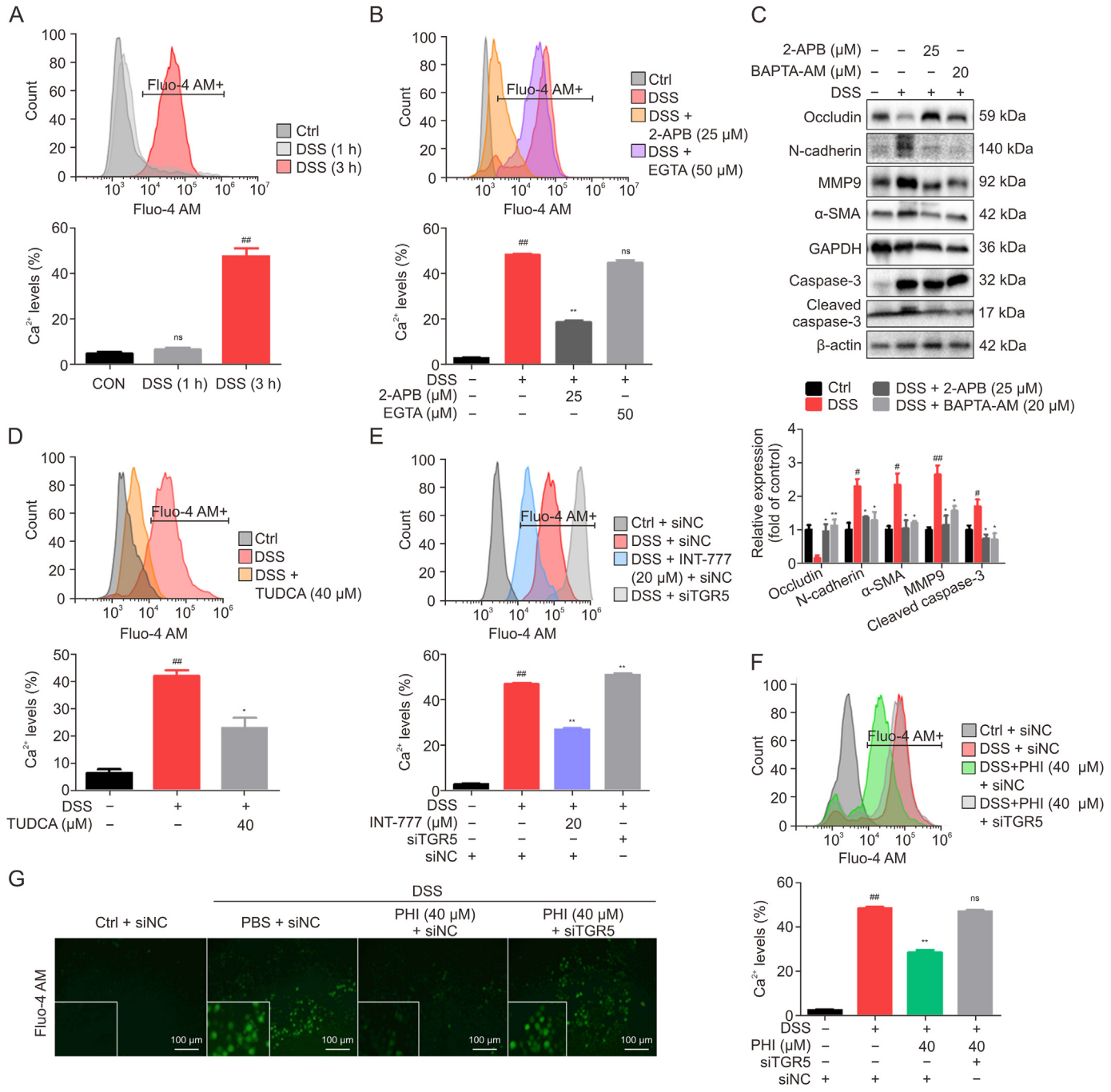

Fig. 9. Phillygenin (PHI) enhanced NCM460 cells function by activating Takeda G protein-coupled receptor-5 (TGR5) to inhibit endoplasmic reticulum stress (ERS)-induced Ca^{2+} release. (A) NCM460 cells were treated with 2% dextran sulfate sodium (DSS) for 1 or 3 h, and then intracellular Ca^{2+} levels were assessed by flow cytometry (FCM) analysis. (B) NCM460 cells were pretreated with 2-aminoethyl diphenylborinate (2-APB) (25 μM) or ethylene glycol tetraacetic acid (EGTA) (50 μM) for 2 h, and then treated with 2% DSS for 3 h; and intracellular Ca^{2+} levels were assessed by FCM analysis. (C) NCM460 cells were pretreated with 2-APB (25 μM) or 1,2-bis-(o-aminophenoxy)ethane-N,N,N',N'-tetraacetic acid tetrakis(acetoxymethyl) ester (BAPTA-AM) (20 μM) for 2 h and followed by 2% DSS stimulation for 24 h; and then occludin, N-cadherin, and matrix metallopeptidase 9 (MMP9) and α-smooth muscle actin (α-SMA) were detected by Western blotting assay, and quantified bands by β-actin or glyceraldehyde-3-phosphate dehydrogenase (GAPDH). (D) NCM460 cells were pretreated with tauroursodeoxycholic acid (TUDCA) (40 μM) for 2 h and followed by 2% DSS stimulation for 3 h; and intracellular Ca^{2+} levels were assessed by FCM analysis. (E, F) NCM460 cells transfected with siTGR5 or siRNA negative control (siNC) before 36 h and treated with 6α-ethyl-23(S)-methyl-3α,7α,12α-trihydroxy-5β-cholan-24-oic acid (INT-777) (20 μM) (E) or PHI (40 μM) (F) for 2 h and followed by 2% DSS stimulation for 3 h; and then intracellular Ca^{2+} levels were assessed by FCM analysis. (G) Representative fluorescent probe images of Ca^{2+} at 3 h. $^{\#\#}P < 0.01$ vs. Ctrl group; $^{**}P < 0.01$, and $^{*}P < 0.05$ vs. DSS group; ns: not significant. ($n = 3$). Ctrl: Control cells.

which was related to the activation of PERK-eIF2α pathway at 3 h. We further confirmed that high levels of cytosolic Ca^{2+} mainly originated from the ER in DSS-induced NCM460 cells. Moreover, 2-APB and BAPTA-AM partially mitigated the DSS-induced TJs reduction, fibrosis, and apoptosis in NCM460 cells. The ERS inhibitor, TUDCA, reduced the elevated intracellular Ca^{2+} as well, suggesting that the PERK-eIF2α pathway activation caused the ER Ca^{2+} release to promoting the NCM460 cell injury. BAPTA-AM and 2-APB treatment also blocked the activation of eIF2α signaling after DSS stimulation for 24 h (Fig. S8). The results suggest that excessive cytosolic Ca^{2+} further exacerbated the PERK-eIF2α pathway, leading to the NCM460 cell damages. We

further explored the role of TGR5 activation in the regulation Ca^{2+} homeostasis in DSS-induced NCM460 cells. INT-777 decreased intracellular Ca^{2+} levels, whereas TGR5 silencing increased the Ca^{2+} levels, indicating that TGR5 activation modulates ER Ca^{2+} release to maintain NCM460 cell function. PHI treatment also markedly reduced the Ca^{2+} levels at 3 h, whereas siTGR5 treatment weakened the inhibitory effects of PHI. These data demonstrate that PHI inhibited the PERK-eIF2α-Ca^{2+} pathway via TGR5 activation to alleviate DSS-induced NCM460 cell injury.

5. Conclusions

In conclusion, the present study confirmed the beneficial effects of PHI against DSS-induced chronic colitis in mice as well as DSS-stimulated NCM460 cell injury, indicating that PHI is a potential and promising therapy for UC. Specifically, PHI treatment substantially improved intestinal TJs reduction, fibrosis, apoptosis, and ISCs activity, indicating a protective effect of PHI on the intestinal mucosal barrier in mice with chronic colitis. In terms of the underlying mechanism, gut microbiota-scondary BAs-mediated TGR5 activation played a partial role in PHI-treated mice with chronic colitis. More importantly, in an *in vitro* model of intestinal epithelial cell injury, PHI intervention directly activated TGR5 to inhibit TJs reduction, fibrosis, and apoptosis, thereby improving NCM460 cell function. Meanwhile, the inhibitory effects of PHI on TJs reduction, fibrosis, and apoptosis were attributed to inactivation of PERK-eIF2α-Ca^{2+} signaling pathway. In summary, our study demonstrated a novel mechanism by which PHI inhibited PERK-eIF2α-Ca^{2+} pathway through the TGR5 activation to improve DSS-induced TJs reduction, fibrosis, and apoptosis damages. Our results provide preliminary experimental evidence for the role of TGR5 activation in inhibiting colitis-associated intestinal fibrosis.

CRediT author statement

Huanhuan Xue: Writing − original draft, Validation, Software, Methodology, Data curation. **Peijie Li:** Validation, Methodology. **Jing Guo:** Methodology, Formal analysis. **Tinggui Chen:** Formal analysis, Data curation. **Shifei Li:** Writing − review & editing, Supervision, Funding acquisition, Data curation. **Liwei Zhang:** Writing − review & editing, Supervision, Resources, Funding acquisition.

Declaration of competing interest

The authors declare that there are no conflicts of interest.

Acknowledgments

This research was supported by the National Natural Science Fund of China (Grant Nos.: 31800293 and 32370422) and Project of Standard for TCM (Grant No.: ZYBZH-Y-JIN-34).

Appendix A. Supplementary data

Supplementary data to this article can be found online at https://doi.org/10.1016/j.jpha.2024.101042.

References

[1] S. Mondal, M. Das, R. Ghosh, et al., Chitosan functionalized Mn_3O_4 nanoparticles counteracts ulcerative colitis in mice through modulation of cellular redox state, Commun. Biol. 6 (2023), 647.
[2] L. Dong, J. Xie, Y. Wang, et al., Mannose ameliorates experimental colitis by protecting intestinal barrier integrity, Nat. Commun. 13 (2022), 4804.
[3] M. Rawat, M. Nighot, R. Al-Sadi, et al., IL1B increases intestinal tight junction permeability by up-regulation of MIR200C-3p, which degrades occludin mRNA, Gastroenterology 159 (2020) 1375−1389.
[4] F. Rieder, C. Fiocchi, Intestinal fibrosis in IBD: A dynamic, multifactorial process, Nat. Rev. Gastroenterol. Hepatol. 6 (2009) 228−235.
[5] N. Rout-Pitt, N. Farrow, D. Parsons, et al., Epithelial mesenchymal transition (EMT): A universal process in lung diseases with implications for cystic fibrosis pathophysiology, Respir. Res. 19 (2018), 136.
[6] G.D. Marconi, L. Fonticoli, T.S. Rajan, et al., Epithelial-mesenchymal transition (EMT): The type-2 EMT in wound healing, tissue regeneration and organ fibrosis, Cells 10 (2021), 1587.
[7] X. Wu, X. Lin, J. Tan, et al., Cellular and molecular mechanisms of intestinal fibrosis, Gut Liver 17 (2023) 360−374.
[8] D. Meng, Z. Li, G. Wang, et al., Carvedilol attenuates liver fibrosis by suppressing autophagy and promoting apoptosis in hepatic stellate cells, Biomed. Pharmacother. 108 (2018) 1617−1627.
[9] W. Lin, C. Ma, F. Su, et al., Raf kinase inhibitor protein mediates intestinal epithelial cell apoptosis and promotes IBDs in humans and mice, Gut 66 (2017) 597−610.
[10] M. Eisenstein, Gut reaction, Nature 563 (2018) S34−S35.
[11] C. Guo, W. Chen, Y. Wang, TGR5, not only a metabolic regulator, Front. Physiol. 7 (2016), 646.
[12] H. Duboc, Y. Taché, A.F. Hofmann, The bile acid TGR5 membrane receptor: From basic research to clinical application, Dig. Liver Dis. 46 (2014) 302−312.
[13] S. Cipriani, A. Mencarelli, M.G. Chini, et al., The bile acid receptor GPBAR-1 (TGR5) modulates integrity of intestinal barrier and immune response to experimental colitis, PLoS One 6 (2011), e25637.
[14] W. Yang, F. Han, Y. Gu, et al., TGR5 agonist inhibits intestinal epithelial cell apoptosis via cAMP/PKA/c-FLIP/JNK signaling pathway and ameliorates dextran sulfate sodium-induced ulcerative colitis, Acta Pharmacol. Sin. 44 (2023) 1649−1664.
[15] G. Sorrentino, A. Perino, E. Yildiz, et al., Bile acids signal via TGR5 to activate intestinal stem cells and epithelial regeneration, Gastroenterology 159 (2020) 956−968.e8.
[16] H. Gao, C. He, R. Hua, et al., Endoplasmic reticulum stress of gut enterocyte and intestinal diseases, Front. Mol. Biosci. 9 (2022), 817392.
[17] D. Qiao, Z. Zhang, Y. Zhang, et al., Regulation of endoplasmic reticulum stress-autophagy: A potential therapeutic target for ulcerative colitis, Front. Pharmacol. 12 (2021), 697360.
[18] S. Zheng, X. Wang, D. Zhao, et al., Calcium homeostasis and cancer: Insights from endoplasmic reticulum-centered organelle communications, Trends Cell Biol. 33 (2023) 312−323.
[19] J. Krebs, L.B. Agellon, M. Michalak, Ca^{2+} homeostasis and endoplasmic reticulum (ER) stress: An integrated view of calcium signaling, Biochem. Biophys. Res. Commun. 460 (2015) 114−121.
[20] R. Gangwar, A.S. Meena, P.K. Shukla, et al., Calcium-mediated oxidative stress: A common mechanism in tight junction disruption by different types of cellular stress, Biochem. J. 474 (2017) 731−749.
[21] H. Zhong, R. Song, Q. Pang, et al., Propofol inhibits parthanatos via ROS-ER-calcium-mitochondria signal pathway *in vivo* and *vitro*, Cell Death Dis. 9 (2018), 932.
[22] Z. Wang, Q. Xia, X. Liu, et al., Phytochemistry, pharmacology, quality control and future research of *Forsythia suspensa* (Thunb.) Vahl: A review, J. Ethnopharmacol. 210 (2018) 318−339.
[23] C. Wang, C. Ma, K. Fu, et al., Phillygenin attenuates carbon tetrachloride-induced liver fibrosis via modulating inflammation and gut microbiota, Front. Pharmacol. 12 (2021), 756924.
[24] H. Xue, J. Li, S. Li, et al., Phillygenin attenuated colon inflammation and improved intestinal mucosal barrier in DSS-induced colitis mice via TLR4/Src mediated MAPK and NF-κB signaling pathways, Int. J. Mol. Sci. 24 (2023), 2238.
[25] J. Guo, J. Tang, B. Wang, et al., Phillygenin from *Forsythia suspensa* leaves exhibits analgesic potential and anti-inflammatory activity in carrageenan-induced paw edema in mice, J. Food Biochem. 46 (2022), e14460.
[26] Y. Li, H. Xiao, D. Hu, et al., Berberine ameliorates chronic relapsing dextran sulfate sodium-induced colitis in C57BL/6 mice by suppressing Th17 responses, Pharmacol. Res. 110 (2016) 227−239.
[27] H.S. Cooper, S.N. Murthy, R.S. Shah, et al., Clinicopathologic study of dextran sulfate sodium experimental murine colitis, Lab. Invest. 69 (1993) 238−249.
[28] S. Ma, M. Ning, Q. Zou, et al., OL3, a novel low-absorbed TGR5 agonist with reduced side effects, lowered blood glucose via dual actions on TGR5 activation and DPP-4 inhibition, Acta Pharmacol. Sin. 37 (2016) 1359−1369.
[29] Y. Yan, M. Shao, Q. Qi, et al., Artemisinin analogue SM934 ameliorates DSS-induced mouse ulcerative colitis via suppressing neutrophils and macrophages, Acta Pharmacol. Sin. 39 (2018) 1633−1644.
[30] R. Wang, W. Wen, Z. Jiang, et al., The clinical value of neutrophil-to-lymphocyte ratio (NLR), systemic immune-inflammation index (SII), platelet-to-lymphocyte ratio (PLR) and systemic inflammation response index (SIRI) for predicting the occurrence and severity of pneumonia in patients with intracerebral hemorrhage, Front. Immunol. 14 (2023), 1115031.
[31] K. Parikh, A. Antanaviciute, D. Fawkner-Corbett, et al., Colonic epithelial cell diversity in health and inflammatory bowel disease, Nature 567 (2019) 49−55.
[32] J. Maul, M. Zeitz, Ulcerative colitis: Immune function, tissue fibrosis and current therapeutic considerations, Langenbecks Arch. Surg. 397 (2012) 1−10.

[33] J.H. Won, J.S. Choi, J.-I. Jun, CCN1 interacts with integrins to regulate intestinal stem cell proliferation and differentiation, Nat. Commun. 13 (2022), 3117.
[34] L. Meran, A. Baulies, V.S.W. Li, Intestinal stem cell niche: The extracellular matrix and cellular components, Stem Cells Int. 2017 (2017), 7970385.
[35] J. Cai, L. Sun, F.J. Gonzalez, Gut microbiota-derived bile acids in intestinal immunity, inflammation, and tumorigenesis, Cell Host Microbe 30 (2022) 289–300.
[36] H. Zeng, S. Umar, B. Rust, et al., Secondary bile acids and short chain fatty acids in the colon: A focus on colonic microbiome, cell proliferation, inflammation, and cancer, Int. J. Mol. Sci. 20 (2019), 1214.
[37] J.A. Winston, C.M. Theriot, Diversification of host bile acids by members of the gut microbiota, Gut Microbes 11 (2020) 158–171.
[38] S. Fiorucci, A. Carino, M. Baldoni, et al., Bile acid signaling in inflammatory bowel diseases, Dig. Dis. Sci. 66 (2021) 674–693.
[39] X. Zhou, L. Cao, C. Jiang, et al., PPARα-UGT axis activation represses intestinal FXR-FGF15 feedback signalling and exacerbates experimental colitis, Nat. Commun. 5 (2014), 4573.
[40] W. Zhou, W. Wu, Z. Si, et al., The gut microbe *Bacteroides fragilis* ameliorates renal fibrosis in mice, Nat. Commun. 13 (2022), 6081.
[41] G. Xie, R. Jiang, X. Wang, et al., Conjugated secondary 12α-hydroxylated bile acids promote liver fibrogenesis, EbioMedicine 66 (2021), 103290.
[42] L. Ding, Q. Yang, E. Zhang, et al., Notoginsenoside Ft1 acts as a TGR5 agonist but FXR antagonist to alleviate high fat diet-induced obesity and insulin resistance in mice, Acta Pharm. Sin. B 11 (2021) 1541–1554.
[43] H. Li, B.K. Wu, M. Kanchwala, et al., YAP/TAZ drives cell proliferation and tumour growth via a polyamine-eIF5A hypusination-LSD1 axis, Nat. Cell Biol. 24 (2022) 373–383.
[44] X. Ke, K. You, M. Pichaud, et al., Gut bacterial metabolites modulate endoplasmic reticulum stress, Genome Biol. 22 (2021), 292.
[45] S. Shu, H. Wang, J. Zhu, et al., Reciprocal regulation between ER stress and autophagy in renal tubular fibrosis and apoptosis, Cell Death Dis. 12 (2021), 1016.
[46] E. Szegezdi, S.E. Logue, A.M. Gorman, et al., Mediators of endoplasmic reticulum stress-induced apoptosis, EMBO Rep. 7 (2006) 880–885.
[47] J. Brooks-Warburton, D. Modos, P. Sudhakar, et al., A systems genomics approach to uncover patient-specific pathogenic pathways and proteins in ulcerative colitis, Nat. Commun. 13 (2022), 2299.